UNIVERSITÀ DEGLI STUDI DI CATANIA
FACOLTÀ DI INGEGNERIA ELETTRICA
ELETTRONICA E INFORMATICA

XXVII cycle Ph.D. in System Engineering

Viviana De Luca

Advanced modeling techniques for electroactive polymers transducers

Ph.D. Thesis

Tutor: Prof. S. Graziani
Coordinator: Prof. L. Fortuna

2014

The Ph.D. activity was granted
by Italian Miur under the project
"PON01_00700 Ambition Power, Formazione"

Contents

Abstract

This dissertation deals with the modeling of electroactive polymers. More specifically IPMCs and IP²Cs, which are electroactive polymers that can be used both as sensors and as actuators, have been considered.

The modeling of IPMC and IP²C transducers, in fact, is an open issue relevant to the development of effective applications. An introductions to the general framework of the proposed models of Electroactive polymers will be given in Section 1, while, in Sections 2 and 3, a multiphysics model of actuators is presented in details. It integrates the description of the electrical, mechanical, chemical and thermal coupled physics domains in a unique solution. As a novel contribution, a model optimization procedure which integrates Nelder-Mead simplex method with the multiphysics model is exploited to identify model parameters by fitting experimental data. A further nonlinear neural network model of IP²C actuators has been implemented and the results will be described in Section 4. The proposed model takes into account the humidity dependence of the device as a modifying input. Three different Neural Network models, e.g. Feed-forward neural network, Radial-basis neural network and recurrent neural network are developed and a comparison of proposed model have been reported.

Modeling of Electroactive transducers

1 Introduction

In these years, intense research has been conducted in order to improve organic materials performance and to develop innovative low-cost fabrication techniques. Organic materials offer the possibility of realizing new devices and applications with unusual properties such as flexibility, lightweight, disposability and eventually bio-compatibility [1]. In this scenario, electro-active polymers (EAPs) are materials, often composites, suitable for realization of innovative transducers, since they have capabilities to transform electrical energy into mechanical energy and vice versa. [2][3].

Thanks to their softness, resilience, and the capability of producing large deformation under a low actuation voltage, EAPs are very attractive for potential applications both as actuators and sensors [4][5][6].

It is widely recognized that, beyond the needing to improve materials performance, the full exploitation of this new technology

requires adequate models especially when EAPs based systems require high precision control, such as, for example, those referring to the realization of biomedical devices or micromanipulators [8]. The modeling of this transducers is an open issue relevant to the development of effective applications.

The Ionic Polymers-Metal Composites (IPMCs) and the Ionic Polymers- Polymers Composites (IP²Cs) are a EAPs can be used both as sensors and as actuators.

IP²Cs represents a direct descendent of IPMCs [7], by replacement of metal electrodes by polymeric ones. While IPMC combine the electro-mechanical properties of ionic polymers' membrane with the conductivity of surface electrodes made of deposited noble metals (platinum or gold) [8], IP²Cs are manufactured through deposition of organic conductor electrodes directly on a ionic polymer membrane. The completely polymeric nature of IP²Cs maintains the electro-mechanical coupling capability, a low required voltage, high compliance, lightness, softness of IPMCs and eventually requires simpler production procedures, lower production costs and it is suitable for the integration in envisaged post-silicon all polymeric smart systems.

Different modeling approaches have been proposed to describe the working principle of IPMC and IP²Cs transducers. The first

approach offers the least amount of insight into the fundamental mechanisms and is referred to as the black box modeling approach. This modeling technique provides a purely empirical model of the transducer, obtained through a series of curve fits based on experimental data.

The grey box approach represents a quite useful choice and it is based on a set of simple equations that describe understood phenomena. These equations are ruled by parameters that are determined by processing experimental data. Provided that such parameters refer to macroscopic properties of the materials, the grey box approach can assure quite general models, useful in the design phase.

The third level of models, called white box or physics-based models, rely on the understanding and description of the physical mechanisms underlying the IPMC (or IP²C) transduction phenomenon to develop a set of equations that fully describe the system response.

This work focuses on the modeling of IPMCs and IP²Cs electromechanical transduction phenomenon, with relevant applications both as actuators or vibrating sensors.

The proposed models are intended to improve the comprehension of such complex devices and can represent a suitable tool for people involved in the study of such transducers.

2 Device geometry

The device consists of an strip working as an actuator and used in the beam configuration: it is mechanically fixed and electrically powered in correspondence of one of the two ends using a pair of copper electrodes, while the other is free to move, in such a away to produce a corresponding deflection (free deflection).

2.1 Geometry

Three different regions (Figure 1) can be identified in the device structure, which are characterized by different physical and chemical properties:

- the central zone consisting of an ionic polymer, Nafion® 117 produced by DuPont™, distributed by Sigma-Aldrich Group [45];

- the surface electrodes made of platinum (IPMC) or Pedot:PSS (IP²C);

- the metal contacts made of copper which, actually, are not part of the transducers, but are required for their working as actuators.

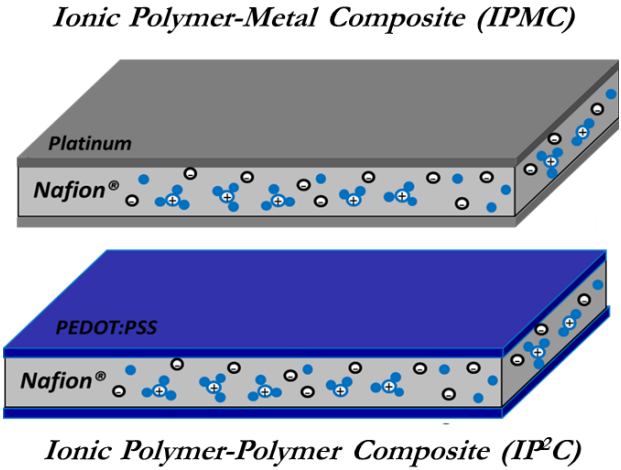

Figure 1: Transducers structure

The geometry of the devices, both for the case of IPMC and IP²C actuators, is shown in Figure 2.

The relevant geometrical parameters are: copper electrode's length L_c=5 mm, total strip length L_t=26 mm, width w=5 mm; thickness of copper, platinum or Pedot:PSS electrodes' and Nafion respectively t_{Cu}=10 μm, t_{Pt}=10 μm and t_{Naf}=180 μm.

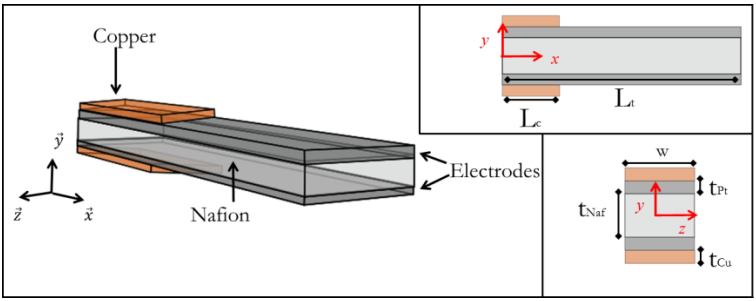

Figure 2: Geometry of the actuators in cantilever configuration

2.2 Manufacturing

In these years, efforts have been also devoted to improve IPMC performances and different problems have been tackled and solved. Among these, the evaporation and electrolysis of water, generally used as the solvent, has been faced with. If water is used as the solvent for IPMCs, they experience water loss and this causes several limitations in terms of performance and applications. If the system works in air, water can be lost both because of its evaporation and of water electrolysis, if the applied electric potential is larger than 1.26 V at room temperature.

These problems can be overcome by using solvents other than water. IPMCs investigated in this work use ethylene glycol (EG) as the solvent, which, like water, consists of polar molecules [48],

avoiding solvent evaporation and allowing larger values of the input voltage, while IP²C use as a solvent the deionized water.

All the polymeric composites considered in this work were kindly furnished by prof.ssa G. Di Pasquale of DII of the University of Catania.

2.2.1 IPMC Manufacturing

Strips of Nafion® 117 films of sizes 3 cm x 4 cm were pre-treated by successive boiling for 30 min in HCl(2N) and deionized water. EG was used as the solvents and platinum as the electrode.

The platinum electrodes were realized by using the electroless plating method. The membranes were immersed for 20 h in a solution of $[Pt(NH_3)_4]\ Cl_2$ (MW = 334.12) obtained by dissolving 205 mg of the complex in 60 ml of deionized water and adding 1 ml of ammonium hydroxide at 5 %. Also, in order to increase the performance of the device, a dispersing agent (polyvinylpyrrolidone with molecular weight 10000-PVP10) was added. $NaBH_4$ was added as reducing agent. Sequential platings (adsorption/reduction) were repeated 3 times. Then the samples were boiled in 0.1M HCl for 1 h. In order to obtain the IPMCs with EG as solvent, water was removed from IPMCs drying the devices at 100°C for 24 h. Then, they were soaked overnight in a beaker containing pure EG and,

finally, heated to 60 °C for 1 h. The obtained membranes were then cut into strips of size 2.6 cm x 0.5 cm.

2.2.2 IP²C Manufacturing

A Nafion® 117 sample (thickness 180 μm and sizes 3 cm x 4 cm) was pre-treated by successive boiling for 1 h in H_2SO_4 (1M), bi-distilled water, 3% H_2O_2 and again in bidistilled water. EDOT (0.426 g, 3 mmol), NaPSS (0.1236 g, 0.6 mmol) and H_2O (160 ml) were stirred at 50°C until a clear solution was obtained. The solution was allowed to cool at room temperature, and a piece of Nafion® 117 membrane was then soaked. Solid $Fe(NO_3)_3$ $9H_2O$ (3.303 g, 7.5 mmol) was then added and stirring was continued for ¼ h. This resulted in a dark blue-black PEDOT-PSS layer being deposited on both sides of the membrane piece. The membrane was then removed from the polymerization solution and well rinsed with bidistilled water. Then the sample was boiled in 1 M H_2SO_4 for 1 h in order to perform the exchanging of Fe^{3+} with H^+ ions, then in H_2O (1 h). Obtained IP²C was then cut in strips of size 2.6 cm x 0.5 cm.

3 Working Principle

The devices transform electrical energy into mechanical reactions and vice-versa, acting both as an actuator and as a sensor. As an

actuator, when an external voltage is applied across the thickness of the IPMC or IP²C, mobile cations (H^+ in the present case) will move toward the cathode. Moreover, when the solvent is dispersed in the polymer sample, the cations will carry solvent molecules with them. The cathode area will expand while the anode area will shrink. If the tip of the strip is free to move, the polymer will bend toward the anode; elsewhere, a blocked force will be delivered. Figure 3 shows how the cations, coupled with the solvent molecules, move towards the cathode and accumulate close to the surface causing the cathode region expansion.

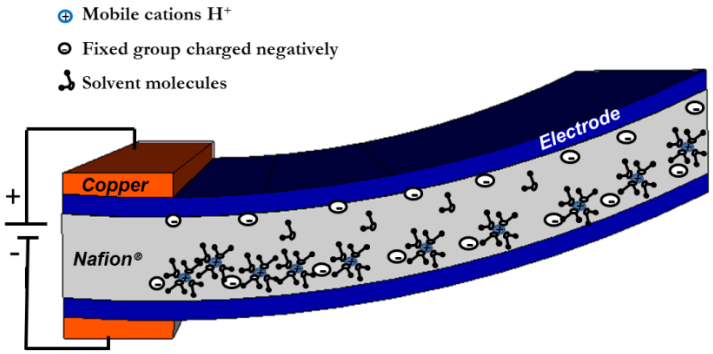

Figure 3: Working principle of an IPMC/IP²C actuator in pinned beam configuration

4 Multiphysics Model

Various approaches have been used in the last decades to describe the physics behind the electro-mechanical transduction of IPMCs and IP²Cs. A taxonomy of physics based models can be found in [9]. According to [9], models can be mainly classified as thermodynamics of irreversible process models, frictional models and Nernst-Planck equation models.

In the first category, approached for the first time by De Gennes in 2000 [10], the mass transport, which is a non-equilibrium thermo-dynamical process, is modeled based on the assumption of local equilibrium. Actually, two different types of models have been developed. The De Gennes model, modified and applied in [11][12][13] and the McGee model [14][15][16]. Both models include the diffusion and the convection fluxes induced by the gradient of the hydrostatic pressure and they are used to qualitatively correlate the deformation, the electrical and mechanical loads.

In the category of frictional models the transport process is described based on the hypothesis that, at steady state, the driving forces are balanced by frictional interactions among various components. The first frictional model to describe IPMCs was introduced by Tadokoro in 2000 [17], where hydrating water molecules moves from the anode to the cathode together with the

cations, driven by the electrostatic force. The electrostatic force is balanced by the frictional force and the diffusion force induced by the concentration gradients. Tadokoro's model was is improved by Toi [18] and Gong [19]. In 2006 Branco proposed a modified transport model [20] but the outcomes disagree with the predictions obtained with the other models. Finally, Yamaue proposed a further frictional model taking into account the contributions of three components, ion, water molecule and polymer network [21].

The NP equation based approach to IPMC and IP²C modeling is at the basis of the white box models developed in this thesis. This group of models is based on Nernst-Planck (NP) equations describing the ion transport in an electrochemical system. It was firstly borrowed by Nemat-Nasser to set a physical model describing the ion flux inside IPMCs in 2000 and 2002 [22][23]. NP equations have been widely applied in the IPMC modeling also by Farinholt [24][25], Chen [26][27], and Choonghee [28] to investigate both the electrically induced deformation (actuator) and the electrical potential induced by the mechanical load (sensor).

NP equations approach has been used by many others in different forms. More specifically, various simplifications have been considered acceptable by Johnson [29] and Pugal [30], Nemat-Nasser [31], Porfiri [32], Aureli [33], Wallmersperger [34], Nardinocchi [35][36] and Zhang [37]. This matter will be further

discussed in the model equations section. The NP modeling is suitable to numerical implementations: the equations can be solved in the form of finite differential equations, by using available software tools.

Other variations on the physics-based approaches exist in literature. Del Bufalo et al. [38] e.g exploit the mixture theory treating the IPMC as the superposition of three species: the polymer backbone, the fluid solvent, and the mobile ions allowing a description of actuation mechanisms, including osmotic pressure, hydraulic pressure, and electrostatic forces. In a further contribution in 2009, Porfiri [39] accounted for fundamental microscopic phenomena, such as electric dipole formation and electrostatic stress generation studied from a micromechanics standpoint.

Literature shows fragmentary efforts in the multi-physics integration for the IPMC and IP^{2}C models including a limited number of coupled physics domains. Most of the electro-chemo-mechanical models have been implemented via numerical methods [41][42], or electro-thermal related phenomena [29]. In other approaches the ion concentration distribution in the IPMC and IP^{2}C boundary layer is mimicked with the temperature distribution, and the electromechanical coupling coefficient is mimicked with the thermal expansion coefficient [43][44].

Based on the consideration reported above, in this thesis a multiphysics model of IPMC and IP²C actuators is developed by using the NP equations. More specifically, a multi-physics model is investigated with the aim to integrate electric, mechanical, chemical, and thermal phenomena involved in the IPMC and IP²C actuators. The proposed model is further implemented by using COMSOL Multiphysics® [40].

Moreover, the proposed modeling approach, while integrating the electrical, chemical, mechanical and thermal physics domains in a single model focusing on the coupling factors, uses the identification of a set of microscopical parameters, by using optimization algorithms in a Comsol Multiphysics®/Matlab® software environment.

The optimization algorithm implemented for parameter identification is a general tool that gives a new methodology for the characterization of new smart materials' properties where the physics parameters are yet not well characterized and sometime difficult to obtain from measurements.

Results are given showing the agreement between multi-physics model simulations and experimental data.

In the following the complex behavior of the actuators, involving chemical, electrical, mechanical and thermal coupled

effects has been modeled using a frequency-dependent multi-physic approach as described in the diagram in Figure 4. It includes four coupled physic models [49][50]:

- **Electrical model** for the study of the electric potential V of the membrane;
- **Chemical model** for the definition of the ionic current and the study of the phenomenon linked to the transport of the solvent;
- **Mechanical model** for determining the deformation of the structure;
- **Thermal model** for determining the temperature distribution on the membrane and its intervention on the ionic transport properties.

The implementation of a unique multi-physics solution is possible thanks to the coupling effects among the different physics domains. In the presented approach the H^+ ionic current density (J) and the electric potential (V) cause interaction between the electrical and the chemical model; the temperature field affects the ionic mobility (μ) and the solvent concentration C_s is the coupling quantity between the chemical and the mechanical model.

In order to reduce the computational load, a 2D model has been considered in the *xy* - coordinates plane. Also the following assumptions on the actuator constitutive materials have been made:

- **isotropy**: the physical properties at every point are the same in all directions and can therefore be represented by scalar quantities,
- **homogeneity**: the physical properties are constant in space for each physics domain,
- **linearity**,
- **time invariance**.

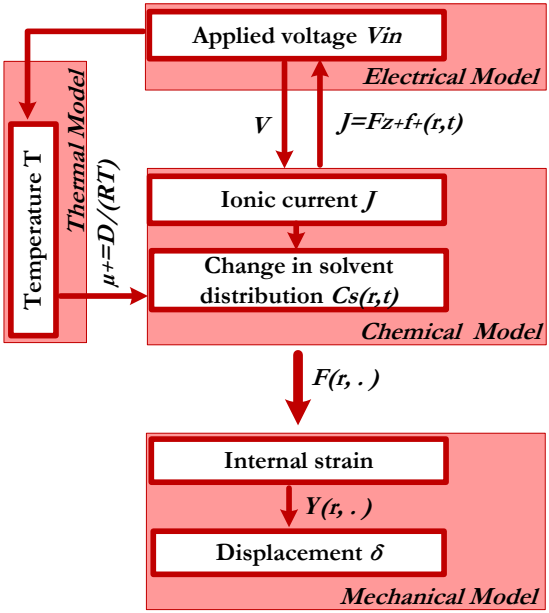

Figure 4: Multiphysics models diagram

4.1 Electrical Model

The electrical and the chemical models are strictly interacting since the applied potential will cause the charge carrier in the Nafion, H^+ ions, to move and therefore to cause ionic current. The equation to be solved in the different physics domains is therefore related to the plane electric current given:

$$-\nabla \cdot \frac{\partial(\varepsilon_0 \varepsilon_r \nabla V(r,t))}{\partial t} - \nabla \cdot (\sigma \nabla V(r,t) - J) = 0 \qquad (1)$$

where ε_0 is the absolute dielectric constant, ε_r is the relative dielectric constant, σ is the conductivity and $V(r,t)$ is the scalar voltage field.

The current contribute $\sigma \nabla V(r,t)$ is given by the electrons flow in each physics domain. J is the cation current density and it represents the coupling factor between the electrical and the chemical model by equation (2).

$$J = F z_+ f_+(r,t) \qquad (2)$$

where F is the Faraday constant, z_+ is the charge number and $f_+(r,t)$ is the total flux of H^+ cations, which is determined by the chemical model through the NP equation.

4.2 Chemical Model

The flux of cations H^+ is linked to the applied potential and to the time variation of the cation molar concentration $C_+(r,t)$ in the undeformed volume. The anion flux is considered null, due to the nature of Nafion. The NP equation (3) rules the cation flux in the actuator [9][23].

$$\frac{\partial C_+(r,t)}{\partial t} = \nabla \cdot \Big(F z_+ \mathrm{u}_+ C_+(r,t) \nabla V(r,t) + D_+ \nabla C_+(r,t) + \mathrm{u}_+ C_+ \mathrm{M}_+ \left(\frac{\mathrm{V}_+}{\mathrm{M}_+} + \frac{\mathrm{V}_S}{\mathrm{M}_S} \right) \nabla p - C_+ \bar{\mathrm{v}} \Big) \qquad (3)$$

where the potential distribution inside the device (V) is calculated in the electrical model solution, D_+ is the cation diffusion coefficient and u_+ is the corresponding mobility, M_+ and M_S are the molar weight of the cations and of the solvent respectively, p is the pressure exerted by the polymer, the convection velocity $\bar{\mathrm{v}}$ is described by Darcy's law (equation 4).

$$\bar{\mathrm{v}} = \mathrm{K}_{\mathrm{EG}} \nabla \mathrm{p} \qquad (4)$$

where K_{EG} is the solvent hydraulic permeability in Nafion117.

The convection velocity was determined by approximating the pressure p exerted on the Nafion in the y-direction as the average y-direction eigen stress given by the mechanical model as suggested in

[58]. Given that the EG molecular mass is higher than the water one, the hydraulic permeability K_{EG} was overestimated by using the $K_{W=}$ 32*10^{-18} (m^2/(s*Pa)) [58]. The y-direction convection velocity results being of the order of $1 * 10^{-12}\mathrm{m/s}$, determining a convection term in the current density J_{conv} of approximately $5 * 10^{-4} A/m^2$. It can be therefore considered negligible with respect to the global current density resulting, from experimental data, of the order of one thousand of ampere per squared meter.

A simplified version of equation (3) is here considered: the diffusion flux caused by pressure gradient is considered negligible as in [31] and the convection term is ignored as in [29],[30][32]-[35],[37]. Such approximation yields to the determination of f_+ as the cations' flux expressed in the following equation

$$f_+(r,t) = -\left(F\, z_+\, \mu_+\, C_+(r,t)\nabla V(r,t) + D_+\nabla C_+(r,t)\right) \quad (5)$$

Moreover, the u_+ is of particular interest since it is a function of the material, of the universal gas constant R and of the absolute temperature (T). It therefore represents the coupling factor with the thermal model. It is calculated as in equation (6)

$$u_+ = \frac{D_+}{RT} \quad (6)$$

The actuation properties are due to the solvent molecules accumulating on the Nafion surfaces in proximity of the platinum electrodes. The time distribution inside the actuator of the solvent molecules is therefore of interest. The solvent motion is both linked to the capability of cations to carry with them a number of solvent molecules equal to the number of solvation n_+ and to the diffusive phenomenon. These considerations yield to the following equation [42]:

$$\frac{\partial C_s(r,t)}{\partial t} = -\nabla \cdot \left(n_+ f_+(r,t) - D_s \nabla C_s(r,t) \right) \tag{7}$$

where C_s is the solvents concentration, D_s is the solvents diffusion coefficient

Considering the reduced 2D model in the *xy*-plane the average value of the variation of C_s with respect to its initial condition C_{s0} has been calculated over the upper and the lower Nafion/Platinum boundary regions (8.a)(8.b).

$$C_{s_{up}}(t) = \frac{1}{L_t} \int_0^{x_{max}} \left(C_s(r,t) - C_{s_0} \right) dx \qquad for\ y = \frac{t_{Naf}}{2} \tag{8.a}$$

$$C_{s_{low}}(t) = \frac{1}{L_t} \int_0^{x_{max}} \left(C_s(r,t) - C_{s_0} \right) dx \qquad for\ y = -\frac{t_{Naf}}{2} \tag{8.b}$$

The solvent maximum concentration will depend on the input frequency. Therefore the model has been considered at different

frequencies evaluating the frequency response of $C_{s_{up}}$ and $C_{s_{low}}$ in terms of their module $A_{up}(f)$, $A_{low}(f)$ and the phase $\varphi_{up}(f)$, $\varphi_{low}(f)$.

4.3 Mechanical Model

The model determining the actuator beam displacement has been implemented using the layer plane strain which is a structural mechanics model for the two-dimensional geometry study, also valid for large deformations [51]. It considers a Rayleigh damping model [52] with mass damping parameter a_f equal to zero due to the negligible mass of the device and stiffness damping parameter β_f to be evaluated by parameters identification algorithms that fit simulation data with experimental results. The equations of motion have been integrated on all subdomains considering elastic materials.

The mechanical load in the cantilever model is due to the solvent molecules motion determined by the electro-chemical model. The variation of the solvent molar concentration C_s, in fact, causes the material expansion and shrinking and therefore a mechanical load applied to the beam [51]. The model will therefore depend on frequency both due to the frequency dependency of the mechanical load and to the frequency dependency of device mechanical properties, such as the Young modulus.

4.3.1 Frequency Dependent Mechanical Load

The mechanical load F applied on the boundaries between the Platinum and the Nafion subdomains has been considered proportional to the variation of the solvent concentration C_s with respect to the initial concentration C_{s0} , similarly to that given in [51][53] .

$$\bar{F} = k_f(C_s - C_{s0})\hat{x} \qquad (9)$$

where k_f is a constant to be identified by using the parameter identification algorithm (see Section 5).

As well know and as verified in the chemical model simulation, the solvent variation has significant values only near the electrodes/Nafion boundaries. The mechanical load has been thus modeled in the frequency domain for the upper and the lower beam electrode-polymer membrane boundaries by equation (10) in terms of modulus (A) and phase (φ) of Cs_{up} and Cs_{low}.

$$\begin{cases} F_{up}(f) = k_f A_{up}(f) e^{j\varphi up(f)} & for\ y = +\frac{t_{Naf}}{2} \\ F_{low}(f) = k_f A_{low}(f) e^{j\varphi low(f)} & for\ y = -\frac{t_{Naf}}{2} \end{cases} \qquad (10)$$

The resulting stress tensor σ is computed by considering the equation (11) as in [53]:

$$-\nabla \cdot \sigma = \bar{F} \qquad (11)$$

4.3.2 Dynamic Mechanical Method (DMA)

The experimental Young Modulus (Y), included in the model, was determined by using the Dynamic Mechanical Analysis (DMA) method [54] at different frequencies [55] and Temperature. DMA determines the mechanical properties of the IPMC sample while it is subjected to a sinusoidal periodic stress [56][57].

The used instrumentation was the Tritec 2000 DMA (Triton Technology Ltd). It consists of a motor to generate a stress sine wave which is transmitted through a drive shaft to the actuator sample and a sensor that measures the resulting strain. The Young modulus is determined as a function of the applied stress and measured strain amplitudes as well as the phase angle between them. In this case, the "tension" configuration has been used as suitable for the analysis of thin films and fibers. The sample is anchored between a fixed clamp at one end and by the drive shaft on the other.

Figure 5: shows the experimental setup for the DMA measurements.

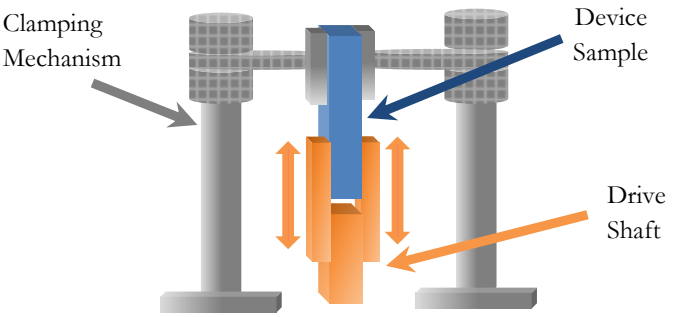

Figure 5: Experimental setup used to measure Young's Modulus.

4.4 Thermal Model

The equation used for the solution of the temperature distribution is the heat transfer by conduction law:

$$\rho C_p \frac{\partial T}{\partial t} - \nabla \cdot (k \nabla T) = Q_T + h_{trans}(T_{ext} - T) \qquad (12.a)$$

$$Q_T \propto \frac{1}{\sigma}(\sigma \nabla V(r,t) - \boldsymbol{J^e})^2 \qquad (12.b)$$

where ϱ is the density, C_p is the specific heat capacity k is the thermal coefficient, T_{ext} is the external temperature and h_{trans} is the convective heat transfer coefficient. Q_T is the heat source: it is affected by the currents, according to the Joule effect as in equation (12.b), and is determined in the electrical model.

4.5 Boundary Condition

Figure 6 shows a schematic of the actuators geometry and accompanying terms that will help to identify the boundary interfaces and corresponding boundary conditions.

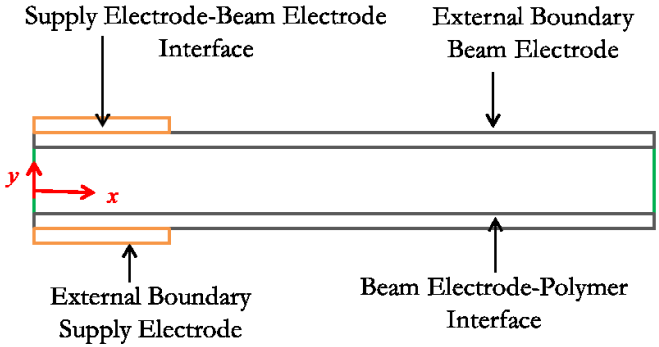

Figure 6:Actuator boundaries

4.5.1 The External boundary supply electrode

The External boundary supply electrode is the location at which an input electrical potential V_{in} is applied to the actuator structure. The required boundary conditions at this interface are:

- Electric Model: $V = V_{in}$
- Chemical model: $C_+ = 0$ (not active in this region)
- Thermal model: $\nabla T = hA(T - T_{amb})$ heat flux
- Mechanical model: fixed

4.5.2 External boundary beam electrode

External boundary beam electrode is the location at which the beam electrode is immersed in air. The required boundary conditions at this interface are:

- Electric Model: $\overline{\boldsymbol{n}}\boldsymbol{J} = 0$ (Electric insulation)
- Chemical model: $C_+ = 0$ (not active in this region)
- Thermal model: $\nabla T = hA(T - T_{amb})$ (heat flux)
- Mechanical model: free

4.5.3 Supply electrode-Beam Electrode interface

In the Supply electrode–polymer interface the variables in all the physics domains models are continuous.

4.5.4 The Beam Electrode-polymer membrane interface

The Electrode-polymer membrane interface is a complex interface. In the electric domain all the variables were approximated as continuous [42]. The concentration variable is discontinuous at this interface, such that the variable C_+ is not active in the electrode region, therefore the cation flux is considered null. Moreover this interface results fundamental for the coupling between the chemical and the mechanical model, since the cation concentration on such

surfaces is considered proportional to the exerted stress (9). At this interface the following boundary condition is used:

- Chemical model: $\overline{\boldsymbol{n}}\boldsymbol{f}_{+} = 0$ insulation condition
- Mechanical Model: the load exerted on this boundary is given by the force due to the cation concentration variation causing the swelling and the shrinking.

5 The Optimization Procedure

Several parameters are generally required in multiphysics modeling in order to describe at a microscopic level the phenomena involved in IPMC and IP²C actuation, some of the parameters used in the models have been identified by using experimental data and fitting model simulations to the devices real behavior. This required to include the COMSOL® based model into a minimization procedure ad-hoc developed by using Matlab™ environment.

The optimization algorithm implemented for parameter identification is a general tool that gives a new methodology for the characterization of new smart materials' properties where the physics parameters are yet not well characterized and sometime difficult to obtain from measurements.

Results are given showing the agreement between multi-physics model simulations and experimental data.

An ad-hoc optimization procedure allowed us to fit the model estimation to the experimental data and to identify model parameters.

In particular the parameters were identified via Nelder-Mead simplex optimization method [59]. Such parameters are strictly related to the technology and to the fabrication process. They are not available as material specifics and they are not directly accessible by experimental measurements.

The parameters identification was performed by comparison of the simulated δ_{sim} and the experimental displacement δ_{exp} of the actuator tip.

The objective function to be minimized was the mean squared error between the simulated and the estimated displacement on N samples: (13).

$$J_{err} = \sqrt{\frac{\sum_{i=1}^{N}\left(|\delta_{exp}(f)|-|\delta_{sim}(f)|\right)^2}{N}} \qquad (13)$$

The optimization algorithm was implemented via a Matlab™ script that uses the *fminsearch* function to search for the minimum of

the scalar function in equation (13), starting at an initial arbitrary value of searched parameters.

The script calls the COMSOL multiphysics model iteratively by changing the design parameter values , according to the *Nelder-Mead* simplex algorithm. The corresponding estimated deflection is produced by COMSOL and used by the minimization algorithm to estimate the current value of the cost function (1). The Procedure is repeated until the tolerance condition $J_{err} < \varepsilon$ is verified (see Figure 7).

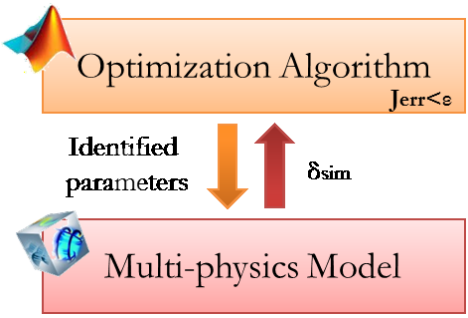

Figure 7: Optimization procedure

6 Experimental Setup

A sine-wave was generated by a signal generator. It was fed into the device through a conditioning circuit cable to generate the current absorbed by the actuator. The dynamic behavior of the

actuator is affected by the relative humidity values, for this reason the measurement surveys were performed into a chamber realized ad-hoc with the aim to control the relative humidity and to measure the environmental temperature.

The environmental temperature T and relative humidity RH% values were measured by using a temperature sensors LM35 and a humidity sensor HiH3610 respectively. The environmental temperature was fixed at the value 25°C, while the investigated humidity range was [40% - 100%].The displacement δ of the free tip was measured by using a distance laser sensor OADM 12U6460/S35A.

The input voltage $V_{in}(t)$ and the corresponding absorbed current $I_{in}(t)$, the environmental temperature, the relative humidity and the device displacement were acquired through an acquisition card DAQ 6052. The system was controlled by using a LabView® VI purposefully developed. In order to investigate exclusively the dependence of actuator behaviors on environmental humidity, acquisitions considered here refer to measurement surveys obtained at a fixed value of the environmental temperature. Values of both relative humidity and the environmental temperature were anyway acquired. The experimental setup is shown in Figure 8.

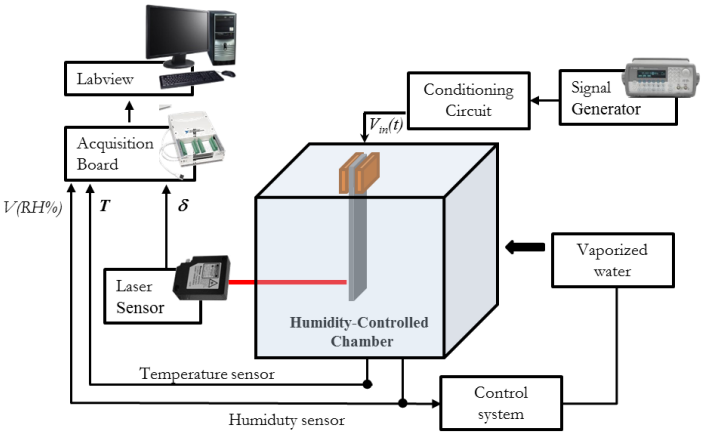

Figure 8: The experimental setup used to investigate the dependence of actuators vibrating behavior on environmental humidity.

7 Multiphysics Model Simulation

As previously stated, the multiphysics model has been solved by using Comsol Femlab. The solver parameters have been fixed as: time-step of $0.2*10^{-3}$ s, absolute tolerance of 10^{-6}. The simulation time for the solution of the model with a single frequency input was 15 min on a Intel(R)Core(TM) i7-3930K CPU @ 3,20 GHz processor with 64GB RAM. In the following some considerations about the results that can be obtained by using the proposed model in the various domains are reported.

Multiphysics models of IPMC actuators

In this chapter multiphysics models of IPMC actuators are proposed is developed. More specifically, a multiphysics model is investigated with the aim to integrate electric, mechanical, chemical, and thermal phenomena involved in the IPMC dynamics. .Such models are implemented by using COMSOL Multiphysics® [44],[56].

Though the models have been described by using the white-box approach resdcibed above, they were ruled by a set of parameters that are not known and that change according to the considered working conditions. Such parameters were determined by using the experimental frequency response $\delta_{exp}(f)$ of the IPMC device displacement, obtained when a swept input voltage stimulus (Vin) with a peak-to-peak amplitude of 4 V and a variable frequency in the range between 1 Hz to 50 Hz was forced to the system.

More specifically the acquired time domain data of the IPMC tip deflection $\delta_{exp}(t)$ were used to estimate the modulus and phase frequency responses by using Matlab™ tools.

1 Parameters Identification considering a full hydrated device (humidity equal to 100%)

In a first case the IPMC model was executed for a fully hydrated device (i.e. with humidity equal to 100%). More specifically, the k_f constant related to the load equation (9) and the stiffness damping parameter β_f in the mechanical model were identified and results were named k_{feff} and β_{feff}. Such parameters are strictly related to the technology and to the fabrication process and they are not available as material specifics neither they are directly accessible by experimental measurements.

In the considered case, the sample number N was 80000, the frequency range is [1 Hz-50 Hz] and the frequency resolution is 0.5 mHz.

1.1 Frequency Dependent of Young Modulus

The experimental Young Modulus (Y), included in the model, was determined by using the Dynamic Mechanical Analysis (DMA) method (see section 0)[54] at different frequencies The measurements were performed at a fixed temperature of 25°C. Low stress was used in order to keep the sample within the elastic region of its stress-strain curve. The curves representing the frequency dependency of both the Storage Young's Modulus and the Loss

Young's modulus of IPMC (Figure 9) were obtained by repeating measurements at different frequencies in the range between 1 Hz and 50 Hz. The experimental storage and loss modulus have been used to take into account the widely reported visco-elastic nature of Nafion [58].

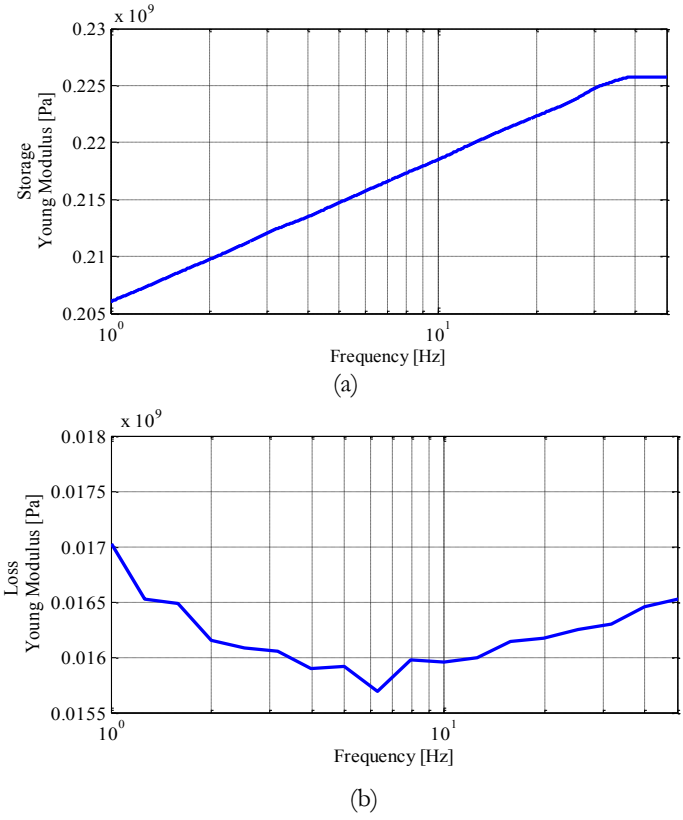

Figure 9: (a)Storage Young's Modulus and (b) Loss Young's Modulus vs frequency of the IPMC actuator

1.2 CASE I: Parameter identification considering a constant Relative dielectric constant ε_r

The parameters used for the COMSOL models are summarized in Table II. The optimal parameters values resulting from the optimization algorithms were: kf_{eff} = 0.041 Nm/mol and βf_{eff} =7.35*10^{-4} s.

TABLE III: SIMULATION PARAMETERS

	Superficial resistance Rs	30 Ω
Electrical model	Nafion electrical conductivity σ	2.16*10 ^{3} S/m
	Copper electrical conductivity σ_{Cu}	58*10^{6} S/m
	Relative dielectric constant ε_r	41.4 F/m
Chemical model	Cations diffusion coefficient D_+	1.4*10^{-9} m^2/s
	Solvents diffusion coefficient D_s	2.4*10^{-12} m^2/s
	Initial cations concentration C_{+0}	1100 mol/m^3
	Initial solvents concentration C_{s0}	2200 mol/m^3

	Number of solvation $\mathbf{n_+}$	2
	charge number z_+	1
Thermal model	Platinum thermal conductivity k_{Pt}	91.7 W/m*K
	Nafion thermal conductivity k_{Na}	0.3 W/m*K
	Copper thermal conductivity k_{Cu}	390 W/m*K
	Platinum density	19600 kg/m^3
	Nafion density	2000 kg/m^3
	Copper density	8960 kg/m^3
	Platinum specific heat capacity	128 J/kg*K
	Nafion specific heat capacity	1870 J/kg*K
	Copper specific heat capacity	380 J/kg*K
Mechanical model	Constant k_{feff}	0.0041 N*m/mol
	Damping parameter β_{feff}	7.35*10^{-4} s

1.3 CASE II: Parameter identification considering Electrodes High Surface

It is well known that the interface between the platinum based electrodes and the polymer presents irregularities and dendritic structures, due to platinum particle penetration within the polymer matrix. It causes an enhancement in the IPMC electric performances and non-homogenous materials properties. Literature presents different models to take into account the roughness of the electrodes of IPMCs. Analytical solutions based on matched asymptotic expansions for the boundary value problem were used by Porfiri [39], while the homogenization of microscopic parameters on the boundary composite layers was introduced by Cha [60][61] in order to obtain IPMC lumped element models. A numerical model was presented by Akle [62] considering conductive particles for the simulation of the Pt absorption in the Pt/Nafion boundary. Moreover a varying-along-the-thickness relative permittivity ε_R is used by Nardinocchi [35] to model the high surface area electrodes. More specifically, ε_R increases on the composite boundaries with respect to the hydrated bulk. In [35] the parameters characterizing the spatial dependency were identified via experimental data. In such approaches, the effects of the electrodes roughness is also approximated with a high effective electric permittivity that can be considered as the spatial average of the of the space-dependent ε_R.

In this case the Platinum/Nafion interface roughness effect has been included in the proposed multiphysics model [67].

The effect of the roughness was considered in the multiphysics model through a varying along the thickness electric permittivity in the y-direction, $\varepsilon_R(y)$.

In particular the $\varepsilon_R(y)$ (Figure 10) function has been chosen as in Nardinocchi [35] with $\varepsilon_{Rmin} = \varepsilon_{EG}$, $\varepsilon_{Rmax} \approx 4.84*10^9$ obtained from the effective capacitance given in [31]. The curve slope was approximated as proposed by Nardinocchi [35] for IPMC with water solvent since the $\varepsilon_R(y)$ parameter is not yet been investigated for the case of IPMCs using EG as the solvent.

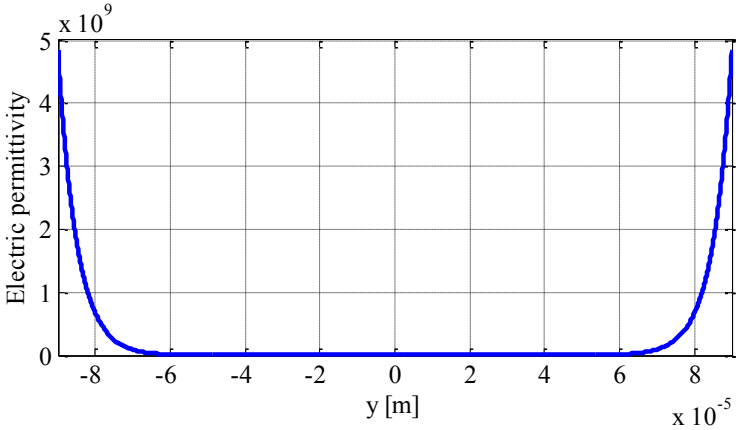

Figure 10: Electric Permittivity along the IPMC thickness.

Considering the electrode high surface, a fractional order dynamics has been identified in the model, confirming previous

studies on IPMC grey box models, confirming previous studies on IPMC grey box model and on electro-active polymeric devices.

The parameter k_f is assumed to be a function of the frequency:

$$k_f(f) = \frac{k_{fo}}{(j2\pi f)^a} \mathrm{k_f(f)} = \frac{\mathrm{k_{fo}}}{(\mathrm{j2\pi f})^{\mathrm{a}}(\mathrm{j2\pi f+p})^{\mathrm{b}}} \qquad (14)$$

The optimal parameters values resulting from the optimization algorithms were: β_f=7.7e^{-4} s and the $k_f(f)$ function was identified as

$$k_f(f) = \frac{0.095}{(j2\pi f)^{0.60}} \qquad (15)$$

The $k_f(f)$ in equation (14) shows a fractional order pole. It demonstrates the IPMC fractional order nature, as already stated for the IPMC grey box models [64][65] and as reported for polarizable polymeric devices, by experimental studies [66].

1.4 CASE III: Parameter identification considering a layered structure

Here a structure closer to real IPMC composition is assumed, since different values of the Young Modulus are taken into account for the bulk Nafion, as obtained by measurement surveys, while the Young modulus of the platinum electrodes was identified by the optimization algorithm. Obtained results reveled a value of the Young modulus of the platinum forming the electrodes smaller than the corresponding value reported in the literature for pure platinum [68]. Such a result is in agreement with the general consensus that IPMC electrodes are not solid but presents a number of cracks that influence the values of both their electrical and mechanical parameters as it will be better discussed in the following.

The constant k_f, the damping parameter β_f and the Platinum Young Modulus Y_{Pt} have been identified by using the optimization algorithm, while the Young Modulus of Nafion was experimentally determined. The curves representing the frequency dependency of Storage Young's Modulus (Figure 11.a) and Loss Young's modulus (Figure 11.b) were obtained by repeating measurements at different frequencies in the range between 1.0 Hz and 45.0 Hz.

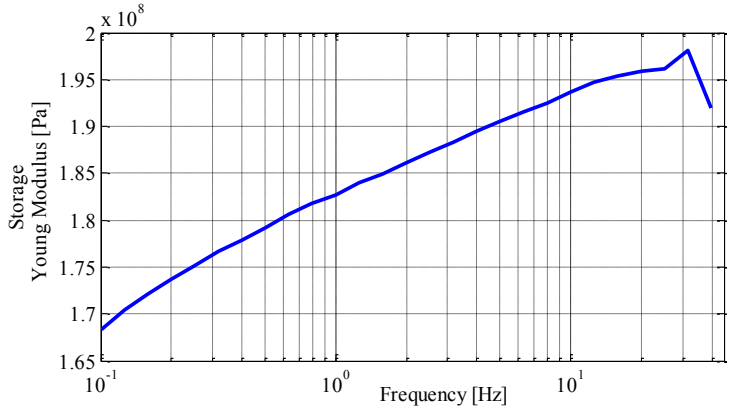

(a)

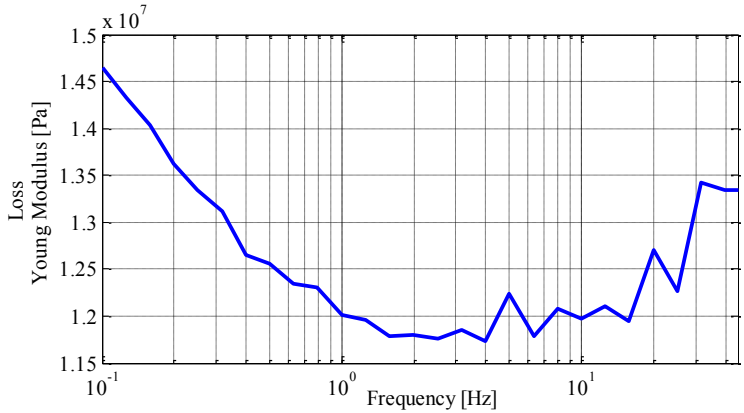

(b)

Figure 11: Storage Young's Modulus(a) and Loss Young Modulus(b) of Nafion.

The parameters used for the multiphysics model, along with the final values obtained for the searched parameters (in bold letters), are summarized in Table IV.

It is worth noticing that, according to the optimization algorithm results, the platinum Young Modulus was identified as 0.98 GPa (see Table VI). This value is by far smaller than the Young Modulus of the pure Platinum as reported in the literature (168 GPa). The obtained result is in accordance with result reported in the literature [63]. In that work in fact the platinum surface resistivity value was about 5000 times larger than the resistivity value reported for plain platinum. The unusually large resistivity value was considered in [63] to be a consequence of the nature of the electrode: the surface of the actuator was porous and the electrode had large cracks. Such a characteristic is also in accordance with a smaller value for the electrode Young modulus, with respect to the pure platinum.

TABLE IV: OPTIMAL PARAMETERS

Parameters	Values
Constant k_f	0.065 N*m/mol
Damping parameter β_f	$84*10^{-4}$ s
Platinum Young Modulus Y_{Pt}	0.98 GPa

2 IPMC multiphysics modeling as a function of relative humidity

The dynamic behavior of an actuator greatly depends on environmental the relative humidity. In this scenario there is a need to implement a models that includes the dependence of the dynamic IPMC behavior on such environmental variable. More specifically, a frequency domain multiphysics model of IPMC actuators is proposed, taking into account the dependence of the device transduction capabilities on the environmental relative humidity. A frequency domain investigation is performed and a model optimization procedure which integrates the simplex method with the multiphysics model is exploited to identify some IPMC model parameters by fitting experimental data.

Compared to models previously described, the proposed one models the direct effect of humidity on microscopic properties of IPMCs.

Such an effect is generally considered as an undesired phenomenon if the actuator is considered, since it introduces a dependence of the system performance on an environmental parameter. Here the aim is to model the dependence of IPMC actuator vibration characteristic. This paves the road to the possibility to use IPMC vibrating structures as humidity sensors.

IPMC actuators in pinned configuration behave in fact as second order under damped systems and reported result show that the humidity values affect both the resonance frequency values and the corresponding resonance peak value, Both these parameters could be used to estimate the environmental humidify value.

A swept sine-wave with a peak to peak amplitude of 4.0 V and a variable frequency in the range between 1.0 Hz to 45.0 Hz ($V_{in}(t)$) was generated by a signal generator. It was fed into the device through a conditioning circuit cable to generate the current absorbed by the IPMC actuator. The environmental temperature was fixed at value 25°C, while the investigated humidity range was [40% - 100%].

The model has been developed by using experimental data and an ad-hoc optimization procedure that allowed to fit the model estimation on experimental data, taking into account the humidity effect.

More specifically, the optimization procedure was required to identify:

- The IPMC Young modulus $\boldsymbol{Y}$
- The constant $\boldsymbol{k_f}$ related to the load equation $\boldsymbol{F(r,f)}$, introduced to transduce the charge accumulation into a corresponding stain.

Table V reports the values of the Young modulus Y and of the coupling term k_f, obtained by using the optimization procedure for all the environmental relative humidity values considered.

TABLE V: OPTIMAL PARAMETERS

Humidity [%]	Young Modulus [GPa]	k_f [N*m/mol]
40	0.49	0.21
60	0.39	0.312
80	0.225	0.15
100	0.18	0.17

3 Simulation Results

In the following some considerations about the results that can be obtained by using the proposed model in the various domains are reported.

3.1 Response to Sinusoidal Signals

An example of the potential field, as the solution of the electrical model, is reported in

Figure 12 [56]. It shows the variation of the potential in the Nafion section between the cathode and the anode. The variation in the *x*-axis direction can also be noticed.

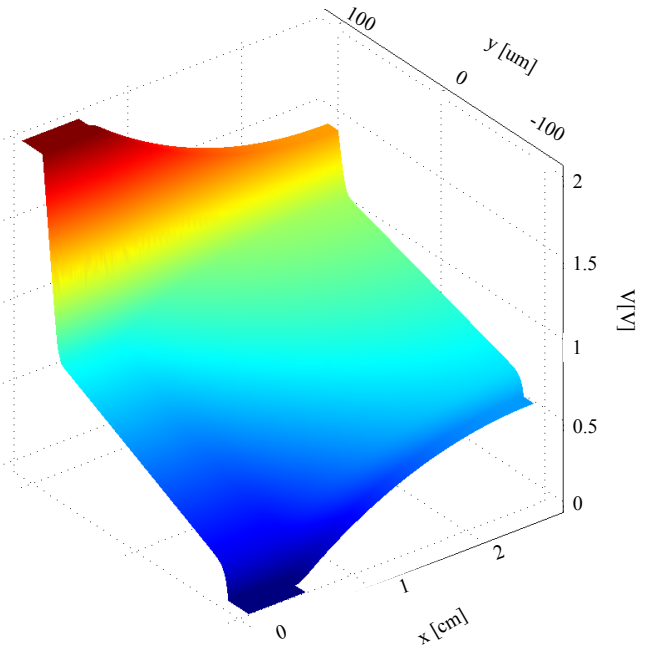

Figure 12: Electric potential V along a IPMC transversal section at simulation time t= 1.25 s (not in scale)

The potential is higher in proximity of the copper electrodes, which provide the input voltage, and decreases in the direction of the IPMC beam tip as a result of the finite values of the copper and

platinum conductivities. The results of chemical model are here presented for a selected input voltage with frequency equal to 1.0 Hz. More specifically, the response to the first sinusoid period is analyzed in order to highlight transient effects. Figure 13 shows that the cationic accumulation and depletion take place only near the boundaries of Nafion to Platinum, while in the central region the concentration is equal to the initial value [56].

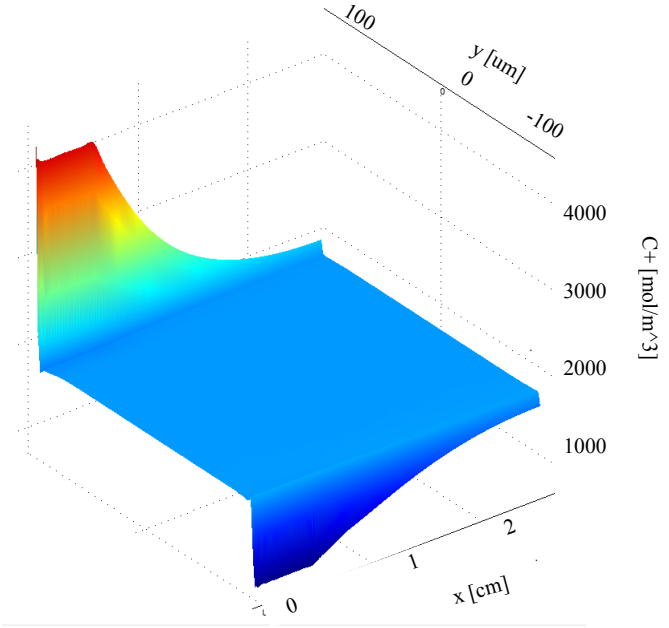

Figure 13: Concentration of the cations C_+ on the Nafion transversal section at simulation time t= 3 s (not in scale).

Note also that the accumulation/depletion phenomena are more evident in the proximity of the copper electrodes. This is again the effect of the finite resistivity of the platinum electrodes.

The concentration changes according to the different polarity of the input voltage. It is worth noticing that, in both the cases, the quantity $C_s(r,t)$-C_{s0} is significant only in an extremely thin region in the vicinity of the upper and lower Nafion/Platinum boundaries: such accumulation and depletion causes the mechanical load as widely reported in the literature.

Figure 15 reports the model solution of the solvent molecules concentration on the Nafion transversal section in correspondence of the $Vin_{(max)}$ (a), and the $Vin_{(min)}$ (b) (see Figure 14)[56].

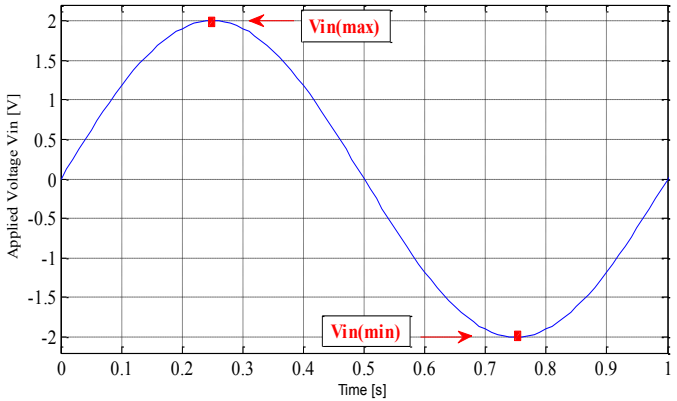

Figure 14: First period of the applied voltage (V_{in}) at the frequency of 1.0 Hz

Figure 15.a represents the simulated solvent concentration response, when the first positive maximum of the input voltage is reached. It shows that the solvent molecules accumulate on the cathode and deplete on the anode, while solvent concentration variation is null within the Nafion section. Figure 15.b, computed in correspondence of the first negative minimum of the input voltage, shows instead a small accumulation of solvent molecules in proximity of the anode and a depletion in proximity of the cathode. It is a transient effect due to the anode-cathode polarity inversion which does not dies out within the input single period, at the considered input frequency [56].

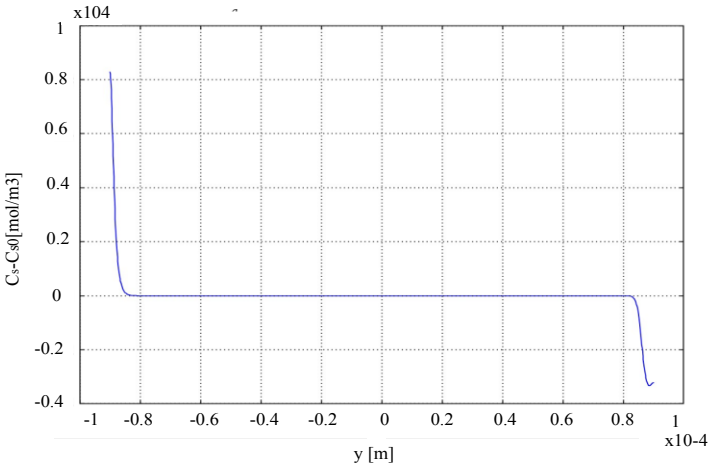

(a)

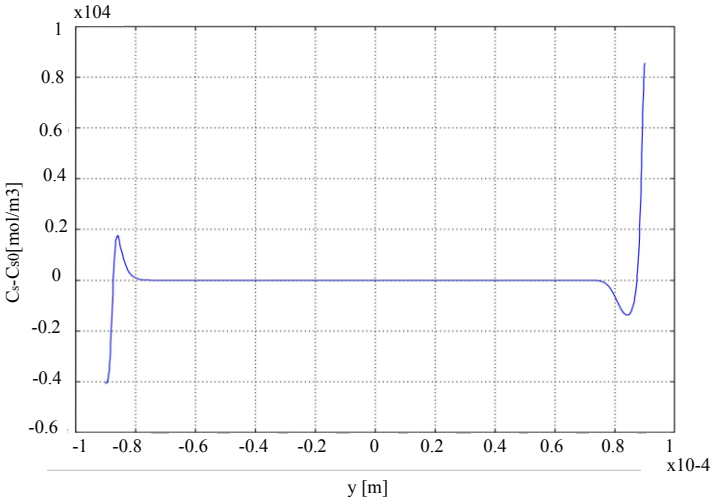

(b)

Figure 15: Variation of solvent concentration in the Nafion section in the first sinusoidal wave at 1Hz at a fixed distance x=0: (a) for $V_{in(max)}$ and b) for $V_{in(min)}$.

Figure 16 reports the model temperature estimation along a IPMC transversal section at simulation time t = 2.5 s. The solution of the thermal model highlights a higher temperature in the central region of the device near the supply electrodes [56].

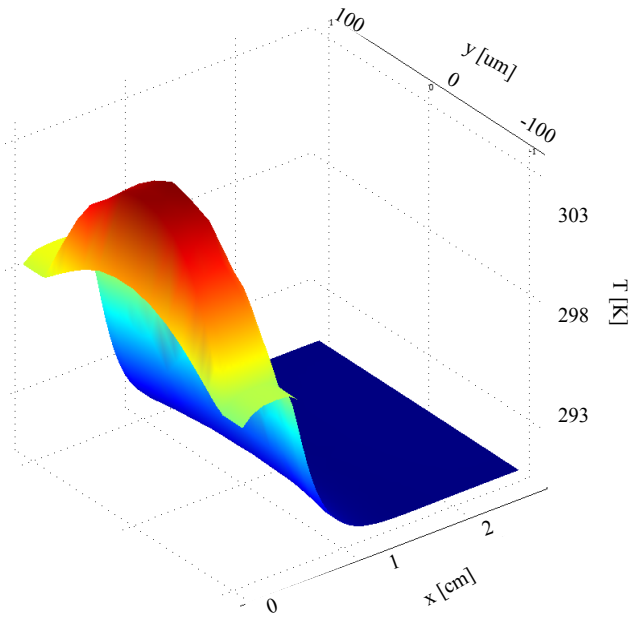

Figure 16: Temperature along a IPMC transversal section at simulation time t= 3 s (not in scale)

3.2 Transient Analysis

In order to better understand the transient phenomenon previously outlined, the transient has been studied by using the analysis of the IPMC response to a square wave input voltage with a time-on (T_{on}) of *20 s* and a following time-off (T_{off}) of *80 s*.

Figure 17 shows the solvent concentration at different instants of the square wave input in order to characterize the accumulation and depletion dynamics in the vicinity of the electrodes during the transient. In particular Figure 17.a shows the behavior at different instant of the T_{on} while Figure 17.b of the T_{off}.

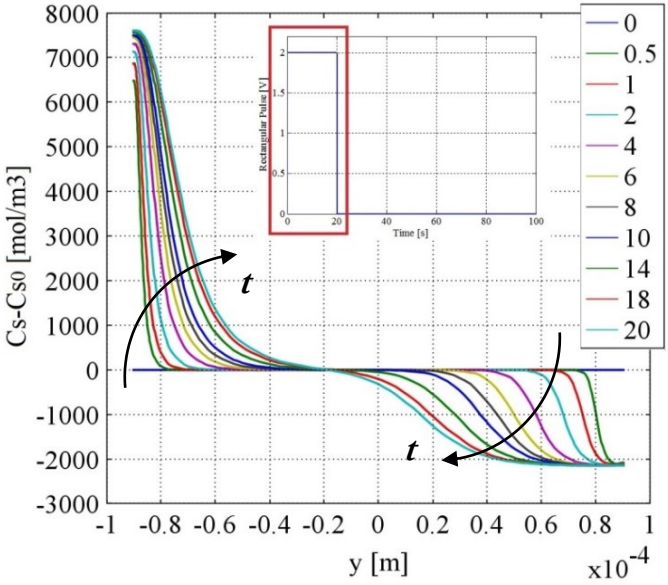

(a)

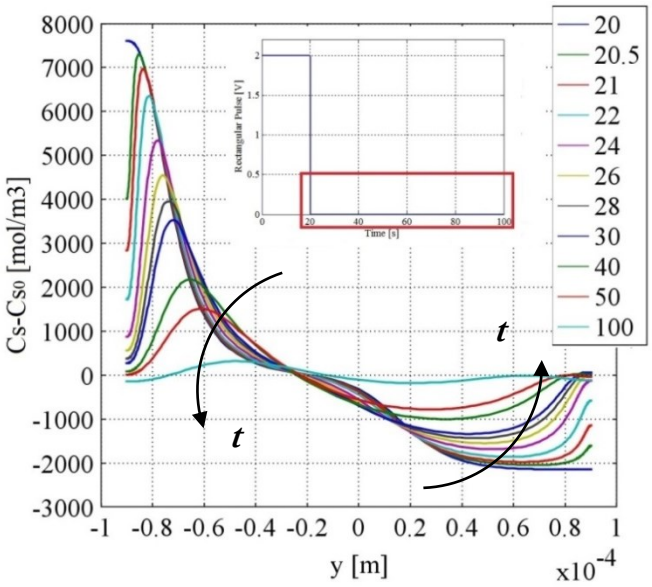

(b)

Figure 17: Variation of solvent concentration in the Nafion section due to a square wave input at a fixed distance x=0: (a) on the T_{on} period, (b) on the T_{off} period.

The accumulation and depletion of the solvent molecules does not occur instantaneously. Instead, it is worth noticing that even after tens of seconds the input signal has been removed a significant charge accumulation has been estimated. Of course, this will have relevant influence on the IPMC actuator tip displacement. The model has been therefore used to estimate, for the considered input

signal, the IPMC deflection. Figure 18 reports the position of the IPMC tip both during the T_{on} (a) and T_{off} (b) intervals.

Inspection of Figure 18.a and Figure 18.b clearly shows a transient mechanical dynamic that compares with the corresponding charge accumulation/depletion dynamics. Also changes in the tip deflection are larger at the beginning of T_{on} and T_{off} intervals, then residual charge accumulations/depletions changes seems to produce smaller effects IPMC tip deflection.

Reported simulation are comparable with the real behavior observed for IPMC actuators with EG as the solvent.

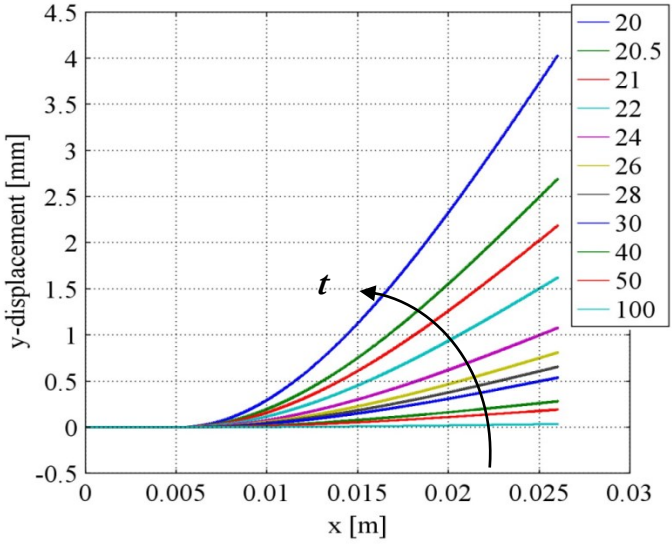

(a)

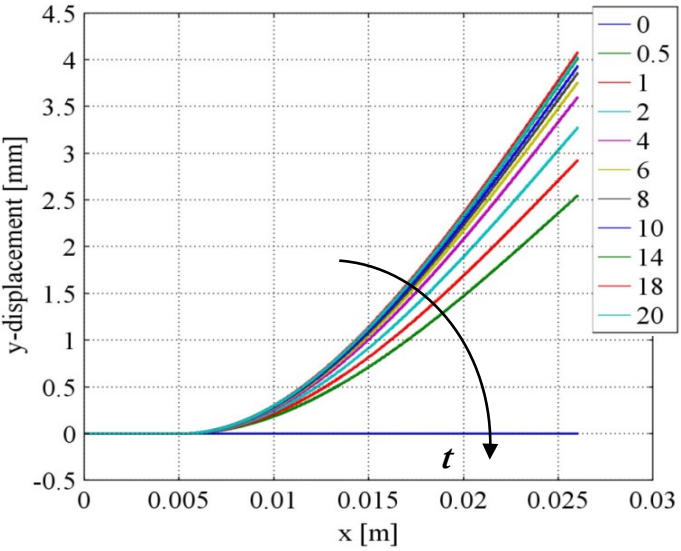

(b)

Figure 18: Variation of solvent concentration in the Nafion section due to a square wave input at a fixed distance x=0: (a) on the T_{on} period, (b) on the T_{off} period..

3.3 Frequency Analysis

In order to study the IPMC frequency response, the integration of the solvent concentration with respect to its initial condition has been integrated on the Nafion/Platinum boundaries as described in equations (8.a) and (8.b) and expressed as $C_{s_{up}}$ and $C_{s_{low}}$ for five input periods.

Figure 19 shows the amplitude of $C_{s_{up}}$ frequency response in correspondence to an input voltage V_{in} at 1 Hz frequency and for a 5 s observation time.

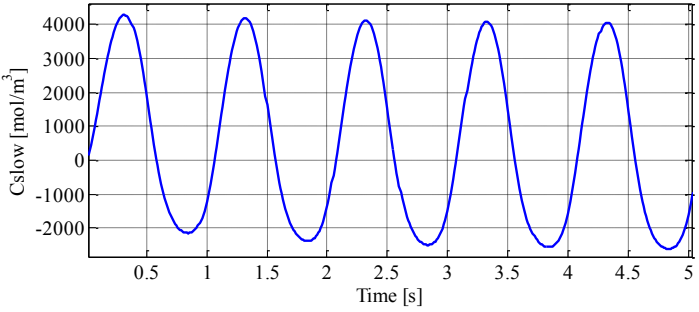

(a)

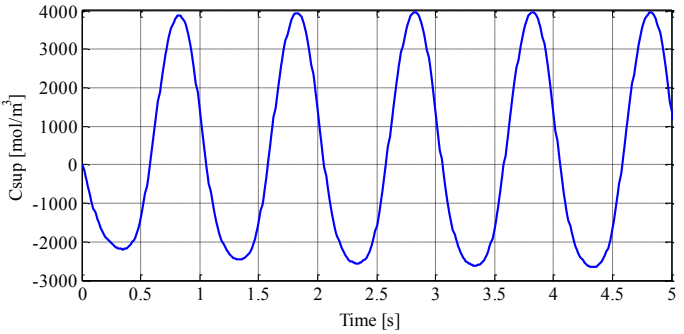

(b)

Figure 19*:* Solvent concentration (Cs-Cs_0) averaged over (a) the upper region and (b) the lower region of Nafion/Platinum boundary.

Moreover, the frequency response of C_{Slow} can be determined by considering the symmetry condition ($A_{up}(f)=A_{low}(f)$, $\varphi_{up}(f)=-\varphi_{low}(f)$) given by the electrical neutrality of Nafion.

Such study has been performed at different frequencies and the solvent concentration frequency response is shown in Figure 20 [56].

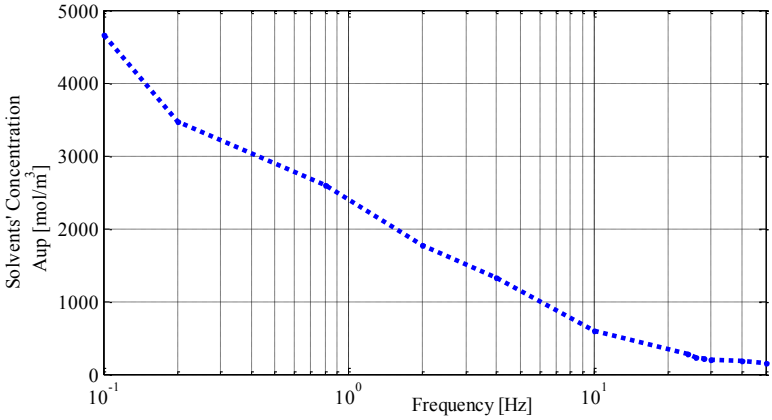

Figure 20: Solvents' concentration vs frequency

Note that the solvent concentration results to be strongly dependent on the applied input frequency.

The resulting frequency dependent solvent concentration presents higher values with respect to the one resulting from a constant $\varepsilon_R = \varepsilon_{EG}$ (see Figure 21) [67].

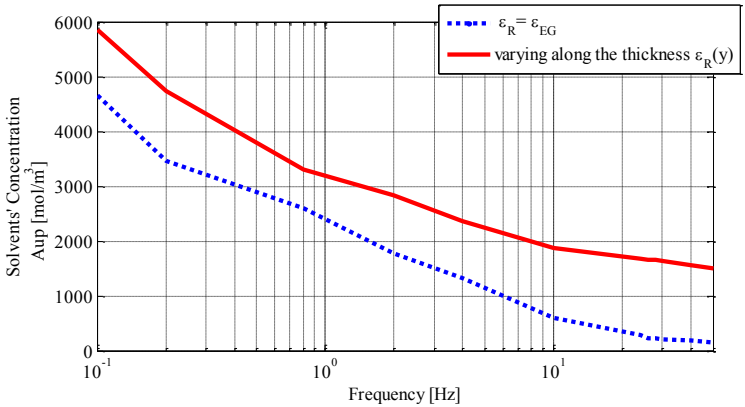

Figure 21: Solvents' concentration vs frequency

Given the cationic accumulation and the results from the mechanical model, it is possible to roughly estimate the convection term of the cation current density J in order to motivate the approximation in equation (2). The convection velocity was determined by approximating the pressure p exerted on the Nafion in the y-direction as the average y-direction eigen stress given by the mechanical model as suggested in [58]. Given that the EG molecular mass is higher than the water one, the hydraulic permeability K_{EG} was overestimated by using the $K_W = 32*10^{-18}$ (m^2/(s Pa)) [58]. The y-direction convection velocity results being of the order of $1*10^{-12}$ m/s, determining a convection term in the current density J_{conv} of approximately $5*10^{-4}$ A/m^2. It can be therefore considered negligible with respect to the global current density resulting, from

experimental data, of the order of one thousand of ampere per squared meter.

4 Models Validation

The validation of the models described so far was executed by comparing experimental and simulated behavior of the IPMC actuator.

4.1 Frequency model validation considering a full hydrated devices (humidity of 100%)

Case I: constant relative electric permittivity. The comparison between experimental and simulated data obtained from the optimized model are given in the following. More specifically, the frequency analysis (displacement/applied voltage) of the device is shown in Figure 22**:** for a suitable frequency range .

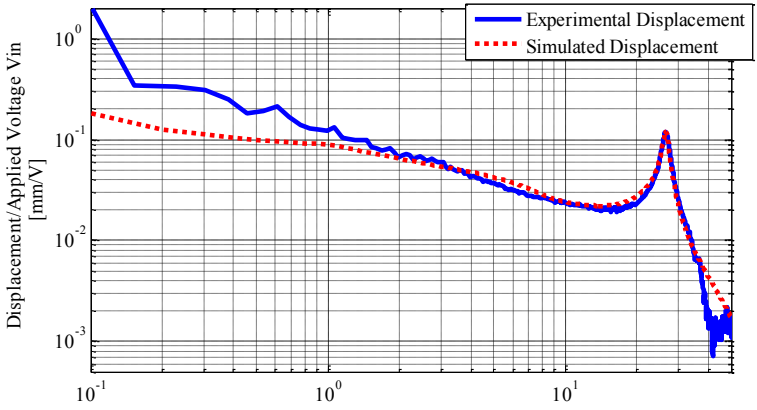

(a)

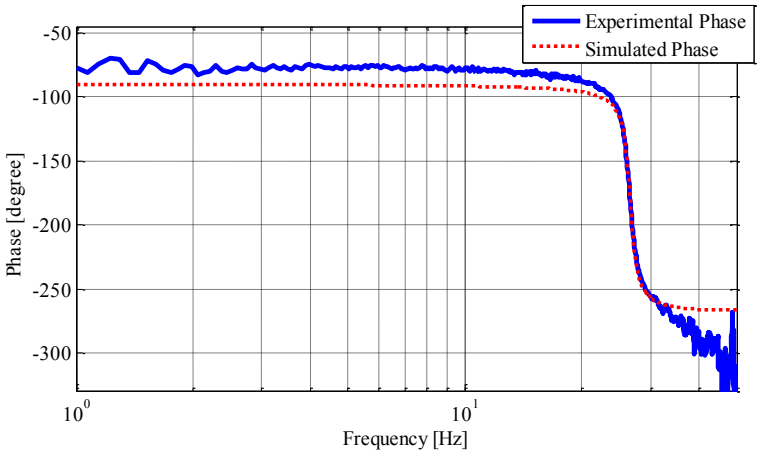

(b)

Figure 22: Comparison between experimental and simulated Frequency response (displacement/Applied voltage):(a)module,(b) phase.

It is worth noticing that the "low pass" like behavior of the IPMC frequency response is consistent with the frequency dependence of solvent concentration reported in Figure 20. On the other hand the resonant like behavior can be associated to the mechanical properties of the device

Case II variable relative electric permittivity in the y-direction. Figure 23 shows the frequency contribute of $k_f(f)$ in terms of module. The phase of the fractional order zero pole results constant at -54° [67].

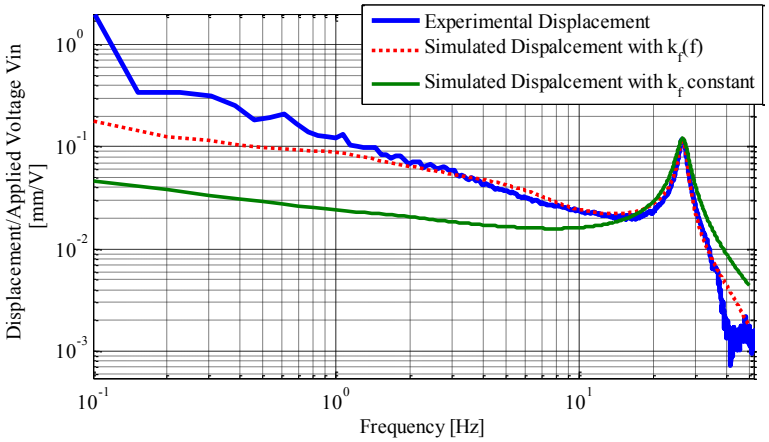

Figure 23: Comparison between experimental and simulated frequency response (displacement/Applied voltage) module

The results allow us to conclude that the optimized model has significant prediction capabilities as regards the actuator frequency response amplitude in the range of interest, highlighting the significant contribute of the frequency dependent $k_f(f)$.

Case III: the layered model: The comparison between experimental and simulated data obtained from the optimized model are given.

More specifically, the comparison between experimental and simulated IPMC deformation obtained from the optimized model is given in

Figure 24. It reports the modulus of the experimental and simulated frequency response (displacement/applied voltage) in the investigated frequency range.

These results allow us to conclude that the optimized model has good prediction capabilities as regards the dynamic actuator behavior in the whole considered frequency range [68].

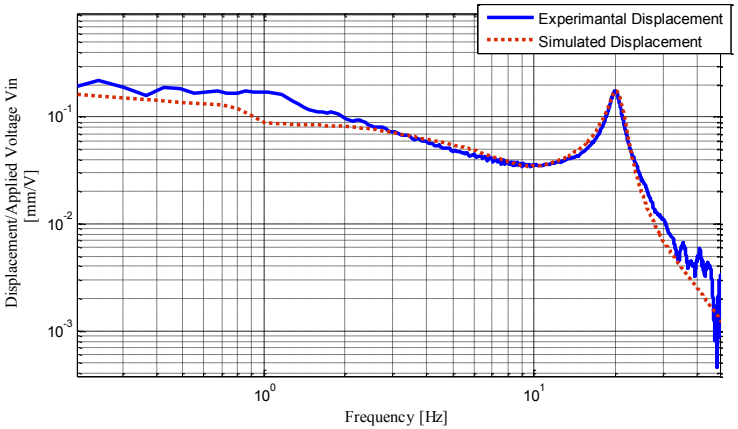

Figure 24: Comparison between experimental and simulated displacements.

4.2 Frequency model validation considering the dependence on environmental humidity

A swept signal was applied to the multiphysics IPMC model, by using the optimized parameters reported in Table V and the corresponding time response was computed. Obtained data were used to estimate the corresponding IPMC frequency response.

The comparison between experimental and simulated data obtained from the optimized model is given in Figure 25 for all considered values of the relative humidity. It reports the

experimental and simulated frequency response (displacement/applied voltage) in the investigated frequency range.

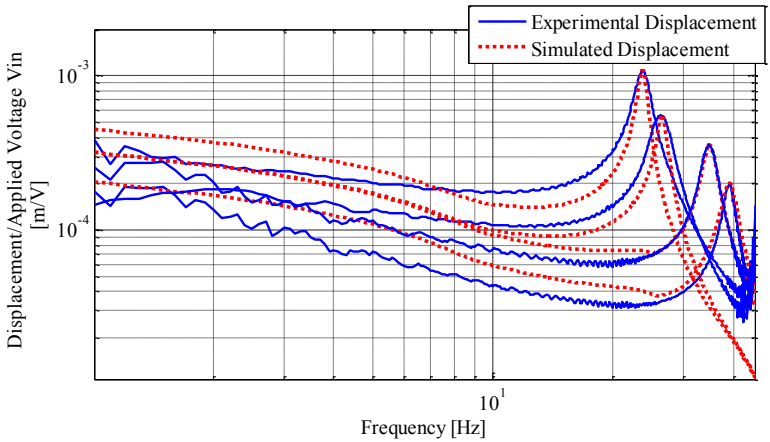

Figure 25: Comparison between experimental and simulated displacements

Though the has poor estimation capabilities both as it regards the very low frequency range response and the shape of the frequency response in the range close to the resonance frequency value [69], reported results show that the obtained model has good estimation capabilities both as it regards the frequency resonance value and the corresponding peak value.

4.3 Time model Validation

Finally, although the optimization algorithm works in the frequency domain, the estimation capability of the models in the time domain have been also investigated. An example of such a validation is reported in Figure 26 where the time response of the model is compared with the corresponding system real tip deflection for the case of a pure tone.

Results described so far allow us to conclude that the optimized model has significant prediction capabilities as regards both the actuator frequency response amplitude and phase, in the range of interest and its time response.

Reported results are in accordance with similar findings reported in the literature and confirm the hypotheses of models based on NP equations. Nonetheless, in the present thesis the white box approach has been further improved by adapting it on experimental data.

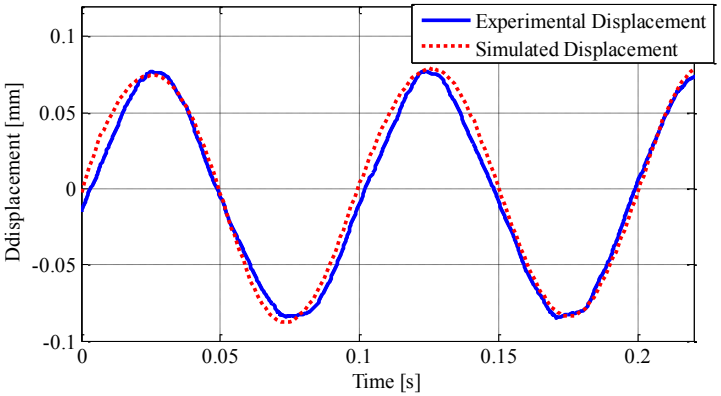

(a)

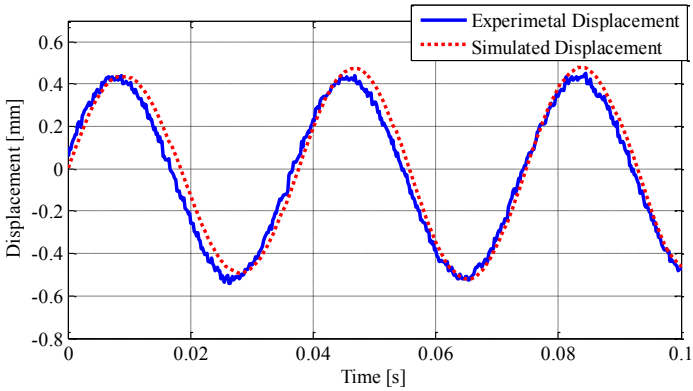

(b)

Figure 26: Comparison between experimental and simulated Displacement versus time using a sinusoidal voltage input with pick to pick amplitude of 4V and a frequency of 10 Hz(a); and a frequency of 26 Hz(b).

Moreover the models allow for the determination of the IPMC actuator frequency response, which is a tool widely used in control design problems. To the best of our knowledge such a strong link between physics-based models and data driven identification was never proposed for IPMC actuators.

Multiphysics models of IP^{2}C actuators

In this chapter moltiphysics models developed for of IP^{2}C will be described in details. Also in this case the models involve electrical, mechanical, chemical and thermal effects and yields a unique solution. Moreover, knowledge acquired by measuring campaigns has been included in the model. More specifically, the frequency dependence of Young's modulus was experimentally determined and introduced in such a model. A frequency domain investigation was performed and a model optimization procedure which integrates Nelder-Mead simplex method with the COMSOL Multiphysics® models was exploited to identify IP^{2}C model parameters by fitting experimental data. As a new result, in this case a a fractional order dynamics has been identified in the model, confirming previous studies on IPMC grey box models and on electro-active polymeric devices. As usual, swept sine-wave, was used also for the investigation reported in this Chapter.

1 Frequency dependence of Young Modulus

The curves representing the frequency dependency of Storage Young's Modulus (Figure 27.a) and Loss Young's modulus (Figure

27.b) were obtained by repeating measurements at different frequencies in the range between 0.1Hz and 50 Hz using the DMA Method [57].

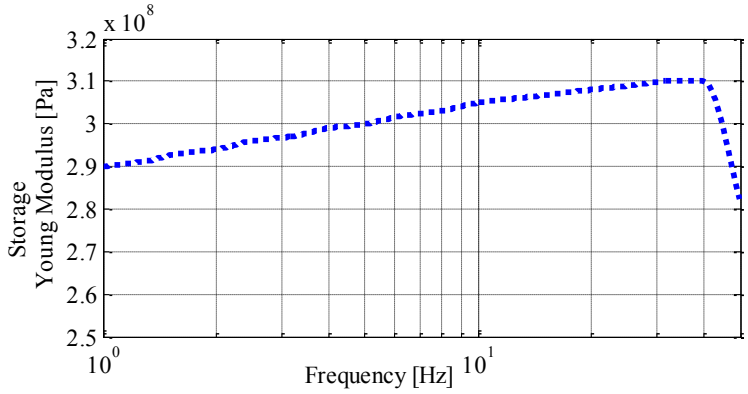

(a)

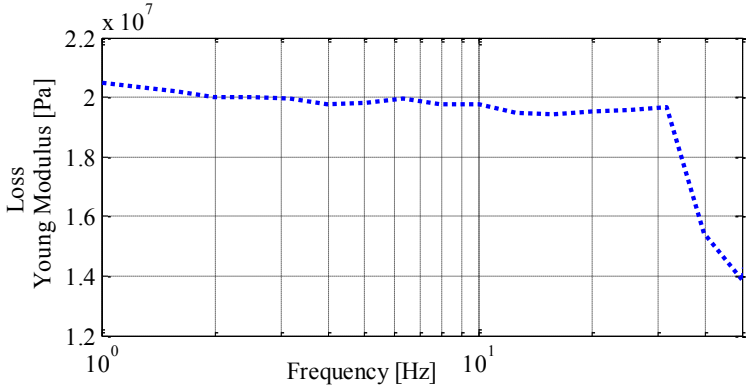

(b)

Figure 27: (a)Storage Young's Modulus vs frequency; (b) Loss Young's Modulus vs frequency.

2 Model Optimization and Parameters Identification

As an original contribute to IP²C modeling, an ad-hoc optimization procedure was developed to fit the model estimation to the experimental data and to identify model parameters.

In particular the parameters k_{f0}, p, a and b of k_f frequency function related to the load equation (9) and the stiffness damping parameter β_f of the mechanical model were identified via Nelder-Mead simplex optimization method. The parameters identification was performed by comparison of the simulated δ_{sim} and the experimental displacement δ_{exp} of the IP²C actuator tip. Data were acquired when a swept sine-wave with a peak to peak amplitude of 4V and a variable frequency in the range between 0.1Hz to 50Hz (Figure 8) was used. Acquired data were further manipulated to estimate the amplitude of the frequency response to sinusoidal input voltage V_{in}.

The following parameters have been used for the optimization algorithm: the termination tolerance (see Section 5) was chosen as $\varepsilon = 10^{-6}$, and the maximum number of iterations was chosen as 100.

A small tolerance has been set in order to force a number of iteration insuring a stable solution. A large maximum number of

iteration was chosen in such a way that further iteration would have not caused any improvement to the optimization performance.

The optimal parameters values resulting from the optimization algorithms were: β_f =1.54e^{-4} s and the $k_f(f)$ function was identified as

$$k_f(f) = \frac{27.08}{(j2\pi f)^{0.62}(j2\pi f+53)^{0.15}} \quad (16)$$

Figure 28.a and Figure 28.b show the frequency contribute of k_f in terms of module and phase respectively [57].

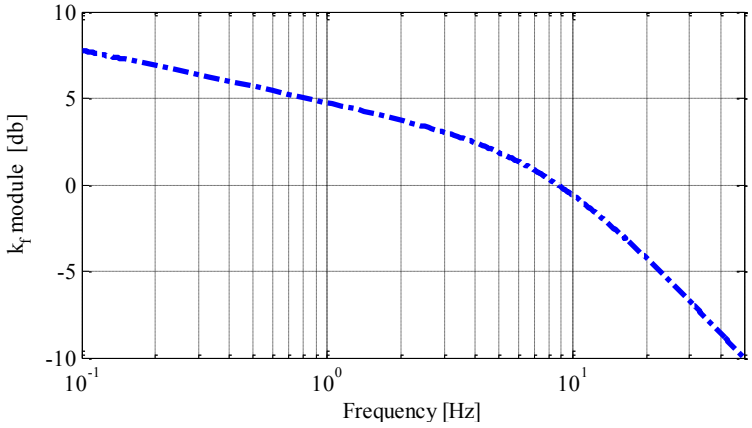

(a)

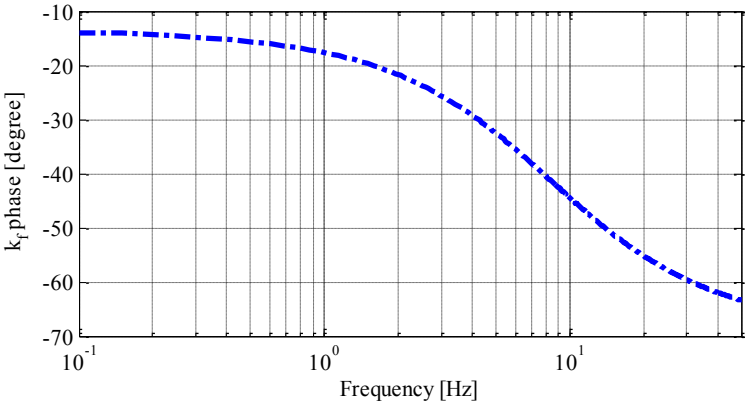

(b)

Figure 28: $k_f(f)$ frequency function in terms of (a) module $|k_f(f)|$ and (b) phase $\Phi_{kf}(f)$.

The $k_f(f)$ in equation (16) shows fractional order poles. This demonstrates the IP²C fractional order nature, as already stated by the authors for the IPMC grey box models [64][65] and as demonstrated for polarizable polymeric devices [66].

The complete set of parameters used to model the IP²C actuator are summarized in Table VI. The term R_s is the superficial resistance and it was experimentally determined. The diffusion coefficients of the cations (D_+) and of the solvent (D_s), were determined experimentally using the capacitive response of the device.

TABLE VI: SIMULATION PARAMETERS

Model	Parameter	Value
Electrical Model	Superficial resistance R_s	60 Ω
	Nafion electrical conductivity σ_{Naf}	$2.16*10^{-3}$ S/m
	Copper electrical conductivity σ_{Cu}	$58*10^{6}$ S/m
	Relative dielectric constant ε_r	81
Chemical Model	Cations diffusion coefficient D_+	$4.9*10^{-11}$ s*mol/Kg
	Solvents diffusion coefficient D_s	$2.4*10^{-10}$ s*mol/Kg
	Initial cations concentration C_{+0}	1200 mol/m^3
	Initial solvents concentration C_{s0}	2400 mol/m^3
	Number of solvation n_+	2
	charge number z_+	1
Thermal Model	Pedot thermal conductivity k_{Ps}	0.23 W/m*K
	Platinum thermal conductivity k_{Pt}	91.7 W/m*K
	Nafion thermal conductivity k_{Naf}	0.3 W/m*K
	Copper thermal conductivity k_{Cu}	390 W/m*K
	Convective heat transfer h_{trans}	30 W/m2*K
	External Temperature T_{ext}	298.15 K
	Pedot density ϱ_{Ps}	1.011 g/cm^3
	Nafion density ϱ_{Naf}	2.5 g/cm^3

	Copper density ϱ_{Cu}	8.96 g/cm^3
Mechanical Model	$k_f(f)$	Eq (14)
	β_f	1.54*10^{-4} s

3 Time Domain Model Validation

The results of electrical, chemical, thermal and mechanical models for the IP^{2}C actuator are here summarized for a selected input voltage (Vin) with frequency equal to 0.2 Hz and peak to peak amplitude of 4 V [50].

The potential field, as the solution of the electrical model at simulation tima equal to 1.25 s, is reported in Figure 29. It shows the variation of the potential in the Nafion section between the cathode and the anode.

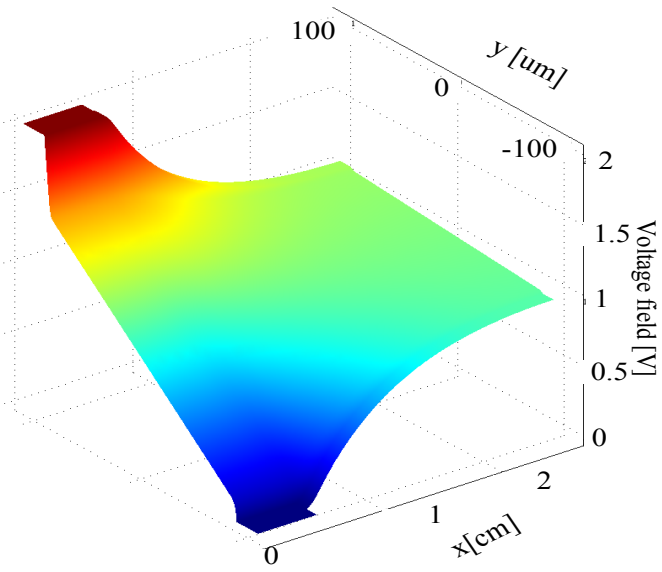

Figure 29: Voltage field (V) on the Nafion transversal section at simulation time t= 1.25 s

The variation in the *x*-axis direction can be also noticed. The potential is higher in proximity of the copper electrodes, which provide the input voltage to the entire device, and decreases in the direction of the IP²C beam tip due to the organic conductor resistivity.

Figure 30 reports the model solution of the cations concentration on a Nafion 2D section at 3 s simulation time. It shows that the cationic accumulation and depletion take place only

near the Nafion boundaries, while in the central region the concentration is equal to the initial value C_{s0}.

The solution of the thermal model highlights a higher temperature in the region closest to the copper electrode, as literature has reported for IPMC [2].

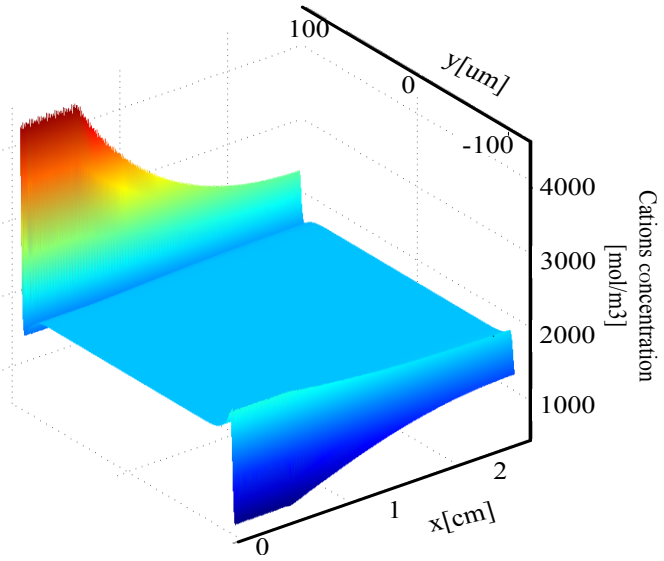

Figure 30: Concentration of the cations (C_+) on the Nafion transversal section at simulation time t= 3 s

The temperature distribution has been investigated in more details and a comparison between the thermal behavior of IPMC.

The temperature distribution has been investigated in more details and a comparison between the thermal behavior of IPMC and IP²C, is reported in the following. Figure 31 shows the temperature trend on a surface section of the Nafion in the x-direction at a fixed y=90 μm for both the IP²C and IPMC excited by the same forcing signal (V_{in}). The higher slope of the IP²C temperature trend is due to the different thermal conductivity of PEDOT:PSS k_{Ps} with respect to platinum k_{Pt} (see Table VI).

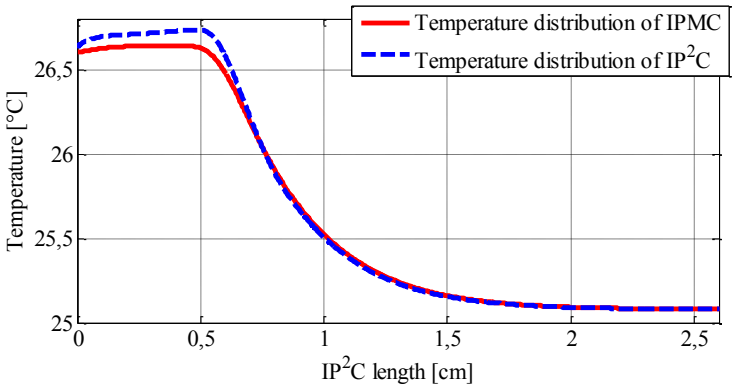

Figure 31: Comparison of thermal performances between IPMC and IP2C: temperature distribution on the x-direction at y=90μm, simulation time t=3 s

Figure 32 shows the comparison between the simulated *y*-displacement and correspondent experimental results, for a given sinusoidal input. The error curve calculated as the difference between experimental and simulated data is presented in order to

state the model performances. Moreover, a resulting correlation coefficient of 98% confirms high correlation between the measured data and the corresponding estimation.

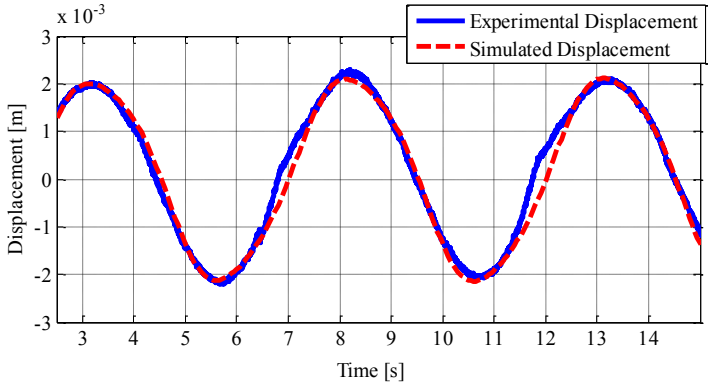

a

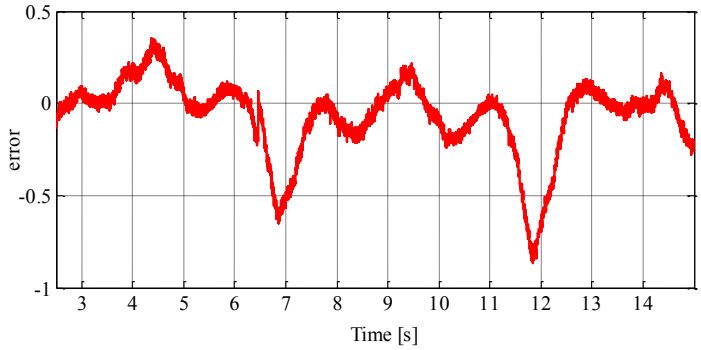

b

Figure 32: a) Experimental and simulation results of displacement in the time domain for sinusoidal input Vin with 4Vpp and frequency f=0.2 Hz, b) error between **e**xperimental and simulation displacement.

4 Frequency Domain Model Validation

A frequency analysis for the IP²C model has been performed in the range between 0.1 Hz and 50 Hz [57].

A preliminary study on the electro-chemical model has been carried out in order to verify how the solvent concentration response, in terms of module and phase, contributes to the overall IP²C mechanical dynamics. Figure 33 reports the Bode diagram module of the solvent concentration on the Nafion/Pedot:PSS boundaries. Due to the hypothesis of linearity, such module trend is consistent with a zero pole system response with fractional order of 0.5. The phase contribute of the solvent concentration response is therefore a delay of -45°.

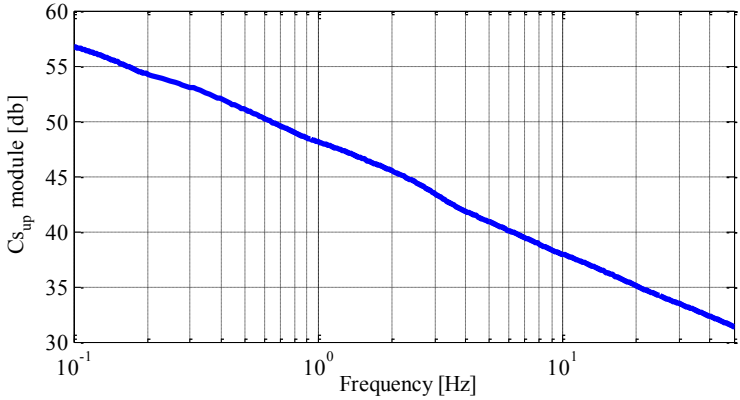

Figure 33: Electro-chemical model result in the frequency domain: $C_{s_{up}}(f)$ module

Moreover the frequency response of $C_{s_{low}}$ can be determined by considering the symmetry condition ($|C_{s_{up}}(f)| = |C_{s_{low}}(f)|$ and $\Phi Csup(f) = -\Phi Cslow(f)$) given by the electrical neutrality of Nafion.

Finally, the comparison between experimental and simulated data obtained from the complete optimized model is given in Figure 34(a) and Figure 35(a). The Figures report the experimental and simulated frequency response (displacement/applied voltage) in the investigated frequency range.

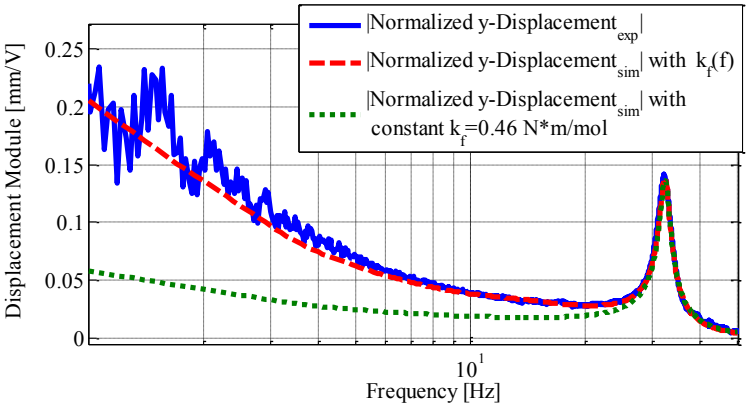

(a)

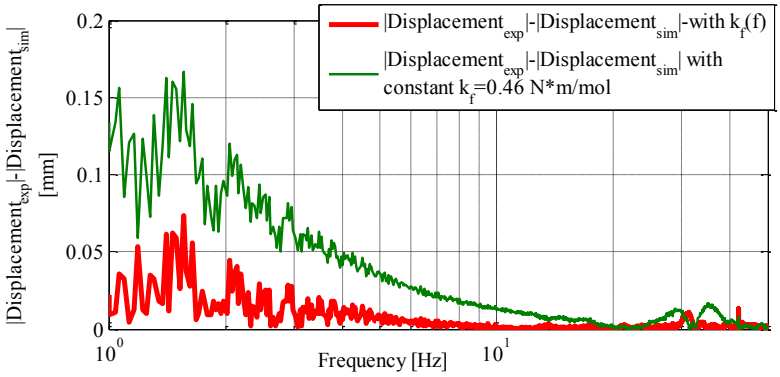

(b)

Figure 34: (a)Comparison between experimental and simulated frequency response (displacement/Applied voltage) module; (b) Difference between experimental(|Displacementexp|) and simulated(|Displacementsim|) y-displacement module

Moreover, the advantage of including the frequency dependence of $k_f(f)$ within the model is here further described. $k_f(f)$ contributes significantly for both the module and the phase in the overall IP²C dynamic response. Figure 34(b) and Figure 35(b) show the differences in the module and the phase between the two cases, i.e. the model with constant k_f=0.46 N*m/mol and the corresponding model, with frequency dependent $k_f(f)$.

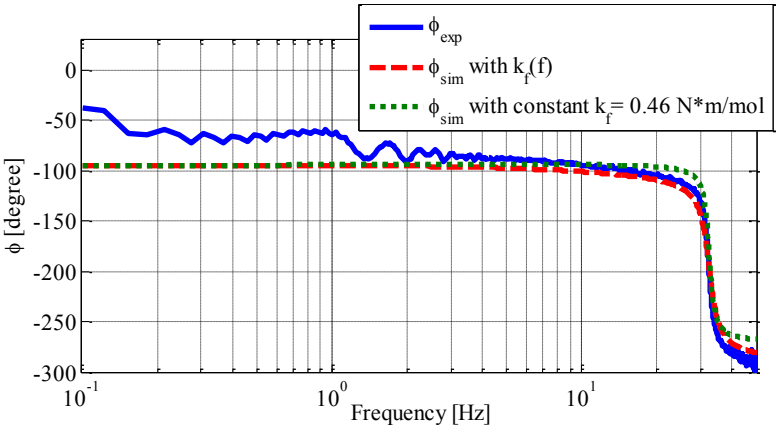

(a)

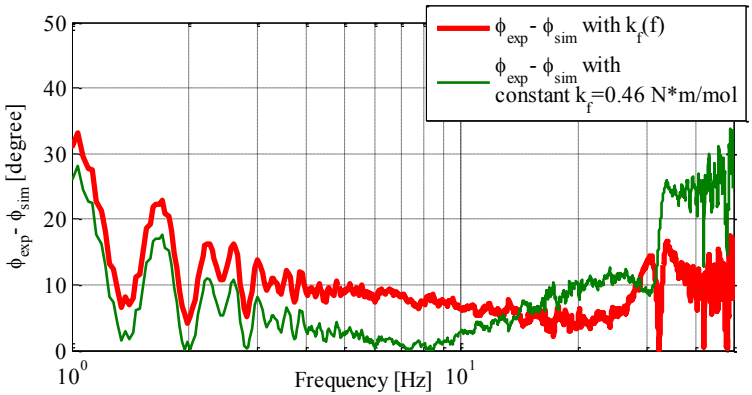

(b)

Figure 35: (a)Comparison between experimental and simulated frequency response (displacement/Applied voltage) phase; (b) Difference between experimental (Φ_{exp}) and simulated(Φ_{sim}) y-displacement phase

These results allow us to conclude that the optimized model has significant prediction capabilities as regards both the actuator frequency response amplitude and phase, in the range of interest. The second order dynamics has been identified with a resonance frequency at about 32.5 Hz.

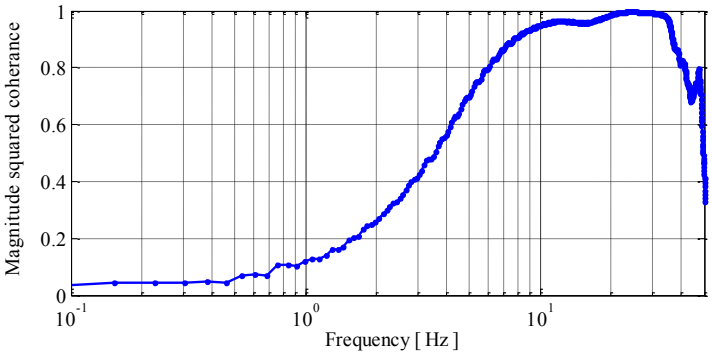

Figure 36: Magnitude squared coherence

Figure 36 shows the magnitude squared coherence between the experimental swept sin-wave input voltage and the output displacement.

The magnitude squared coherence estimate is a function of frequency with values between 0 and 1 that indicates how well the input corresponds to output at each frequency.

The results indicates that at low frequencies, between 0.1 Hz and 10Hz, the coherence between the experimental input and output is

low. Therefore the difference between the experimental and the simulated frequency response in such a frequency range is not considered relevant.

Neural Network Modeling

In this section a model of IP²C actuators, by using the Neural Network modeling will be presented. The model has been developed in the frequency domain. More specifically, the activity focused on the investigation of IP²C dynamic behavior in the frequency domain and the effect of humidity is considered in the modeling [70][71]. The activity reported in this Chapter is the result a of a research activity that I developed during a period of three months that I spent at University of Louisville, under the guide of prof. J.M. Zurada, as part of my PhD program.

In order to develop a model capable to describe the dependence of the device on the value of the humidity, experimental data were acquired from the device, then three different Neural Network models, e.g. Feed-Forward Neural Network, Radial-Basis Neural Network and Recurrent Neural Network were developed. Finally, the obtained models are compared in terms of accuracy [72].

1 Neural Networks

Neural Network is an information processing paradigm that is inspired by the biological nervous systems. It is composed of a large number of highly interconnected processing elements (neurons)

working in union to solve specific problems. Neural Networks can be configured for a number of different applications, such as pattern recognition or data classification, through a learning process. In this work, three different Neural Network models (FFNN, RBNN and RNN) have been investigated.

1.1 Feedforward neural networks

FeedForward Neural Network (FFNN) was the first and arguably most simple type of artificial neural network devised. In this network the information moves in only in the forward direction. From the input nodes data go through the hidden nodes and to the output nodes. There are no cycles or loops in the network.

Assuming a three layer neural network with *n* input nodes, *m* nodes in the hidden layer, and one node in the output layer, the overall response function *f(**x**)* has the following form (equation 17):

$$f(\boldsymbol{x}) = \sum_{i=1}^{m} a_i \, \Omega(\boldsymbol{w}_i \boldsymbol{x}) \qquad (17)$$

where $\boldsymbol{x} \in R^{n\times 1}$, $a_i \in R, \Omega$ is the activation function, and $\boldsymbol{w}_i \in R^{n\times 1}$ is the input weight vector belonging to i-th hidden node [73].

1.2 Radial Basis networks

A Radial Basis Network (RBNN) is a typical three-layer feed forward network that consists of an input layer, a hidden layer with a non-linear Radial Basis activation function, and an output layer [74].

The input can be modeled as a vector of real numbers $\boldsymbol{x} \in R^{n\times 1}$. The output of the network is then a scalar function of the input vector and is given by equation (18):

$$f(\boldsymbol{x}) = \sum_{i=1}^{m} a_i \, \Phi\left(\frac{\|\boldsymbol{x} - \boldsymbol{c}_i\|}{\sigma_i}\right) \tag{18}$$

where m is the number of nodes in the hidden layer, $\boldsymbol{c}_i \in R^{n\times 1}$ and $\sigma_i \in R^{+}$ are the centroid and smoothing factor of the i-th radial basis function, and a_i is the connecting weight of the i-th hidden node to the linear output node. In this work, the Gaussian function was used as the radial basis function $\Phi(.)$ (equation 19):

$$\Phi(\boldsymbol{x}) = \exp\left(\frac{\|\boldsymbol{x} - \boldsymbol{c}_i\|}{\sigma_i}\right) \tag{19}$$

where β is the real constant.

1.3 Recurrent Neural Networks

Recurrent Neural Networks (RNNs) are dynamical systems with temporal state representations [75]. They are computationally powerful, and can be used in many temporal processing models and applications. In this type of neural network, feedback connections between neurons are allowed, and locally recurrent, so that globally feedforward networks with dynamics realized inside neuron models are realized. The recurrent networks, locally, are designed with dynamic neuron models which contain inner feedbacks, but interconnections between neurons are strict feedforward ones, as it is shown in the Figure 37.

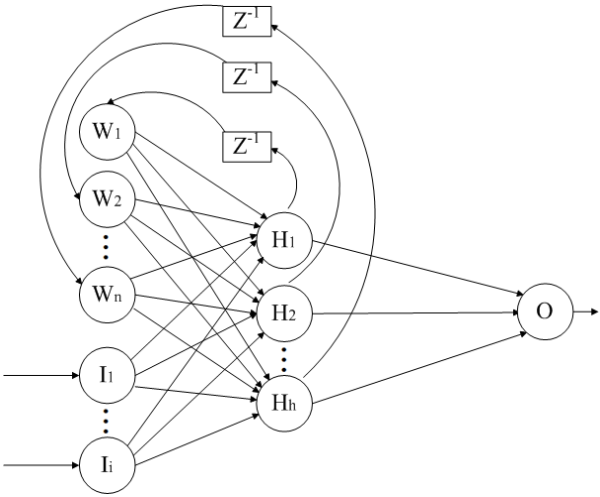

Figure 37: Lean performance of the Network using Feedforward NN.

2 The neural model of the IP²C

Acquired data have been used to identify the IP²C model. More specifically the 70% of the date have been used for the network train and the 30% for the model validation. FFNNs, RBFs and RNNs have been investigated and the comparison of the obtained reslts is reported in the following.

The frequency and the relative humidity are used as inputs and the frequency response as output. Figure 38 shown the inputs and output data, respectively.

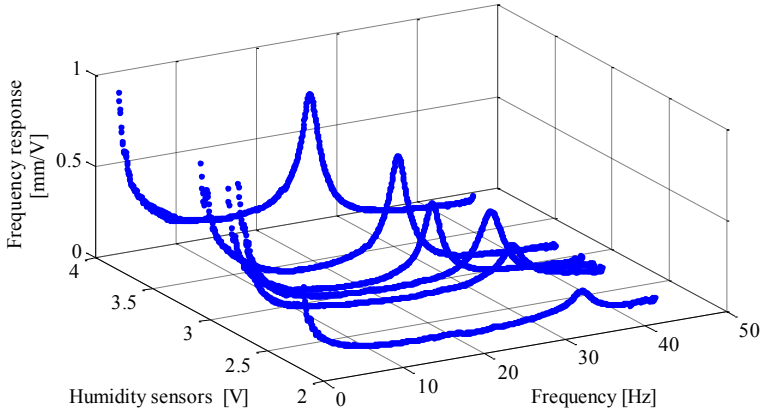

Figure 38: Inputs data for NN models

Firstly FFNN models have been implemented. After a trial and error procedure it was found the best working network had one

hidden layer with 37 neurons, sigmoidal activation functions and a linear output layer. Figure 39 reports the comparison between simulated and experimental output and the corresponding model estimation error.

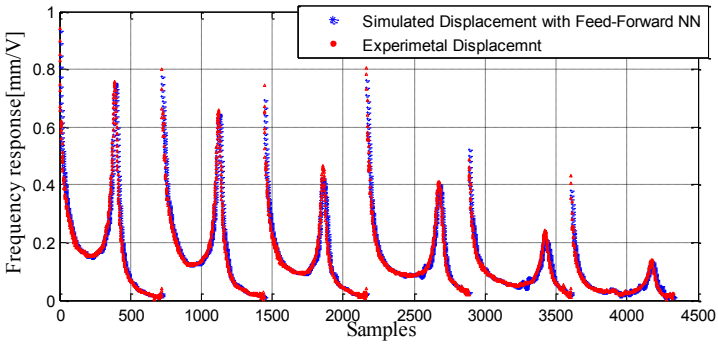

(a)

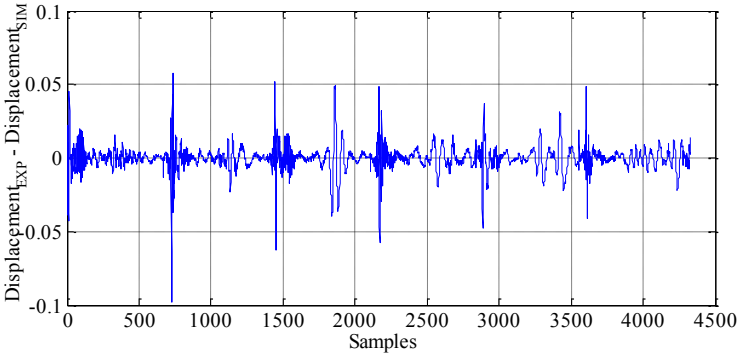

(b)

Figure 39: Comparison between experimental and simulated displacement using FFNN (a) and the corresponding model residue (b).

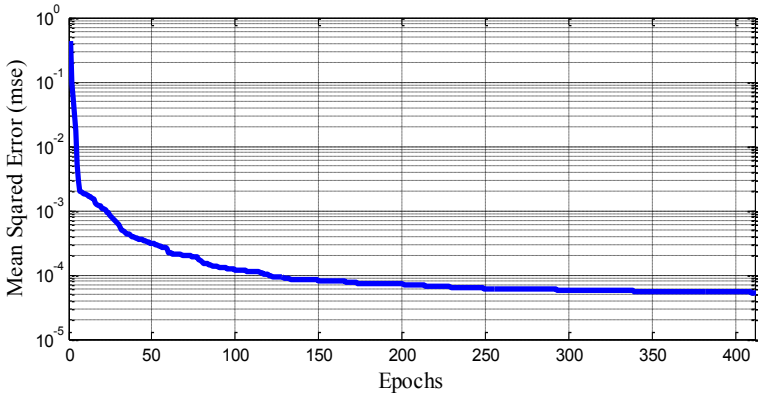

Figure 40: Lean performance of the Network using a FFNN.

The Figure 40 shows the learning performance of the best network with a mean square error of 0.535 $*10^{-4}$ and the epoch number of 411.

The best RBNN had 100 hidden neurons. Figure 41 shows the comparison between simulated and experimental displacement and the corresponding modeling error.

The resulting mean squared error is $0.395*10^{-2}$.

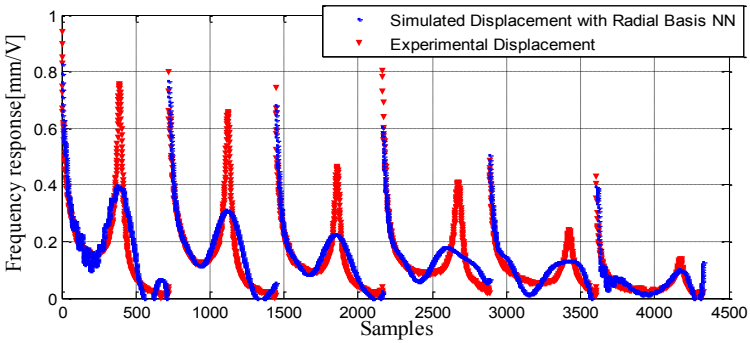

(a)

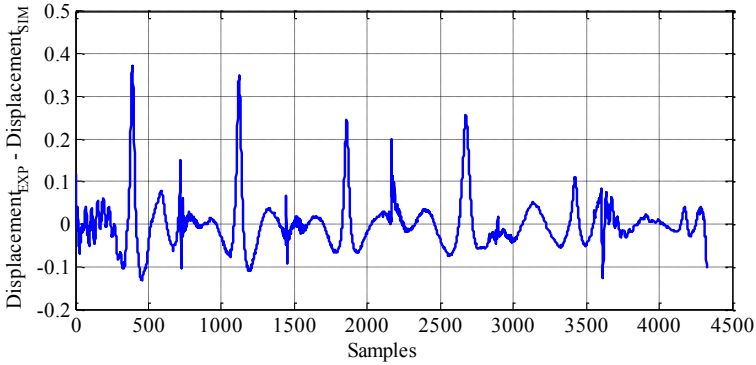

(b)

Figure 41: Comparison between experimental and simulated displacement using RBNN (a) and the corresponding residue (b).

Finally, a Neural Network model with the recurrent architecture has been implemented. The best RNN had one hidden layer with 45

neurons with a sigmoidal activation function, furthermore to improve the training, a delay of one sampling time has been used.

The comparison between experimental and simulated data obtained from the recurrent neural network is given in the following (Figure 42), along with the corresponding model error.

The mean squared error is $0.628*10^{-4}$ and the epoch is 1000, as Figure 43 shows.

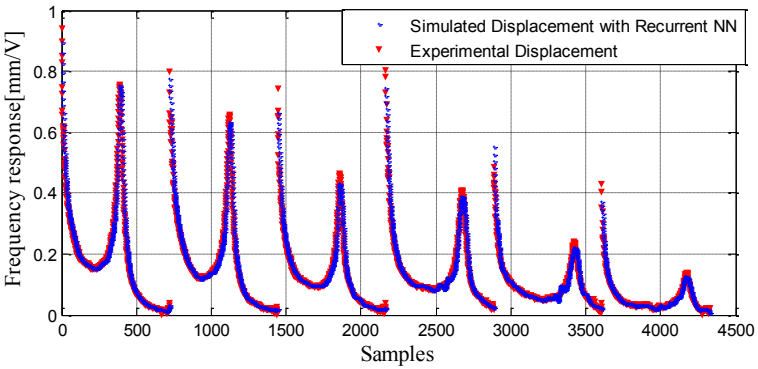

(a)

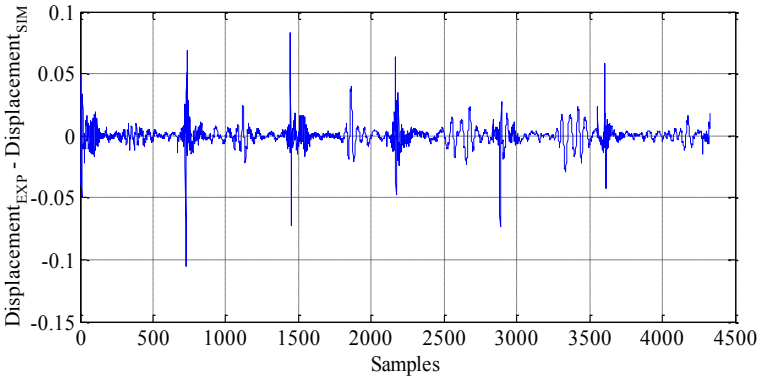

(b)

Figure 42: Comparison between experimental and simulated displacement using RNN (a) and the corresponding residue (b)

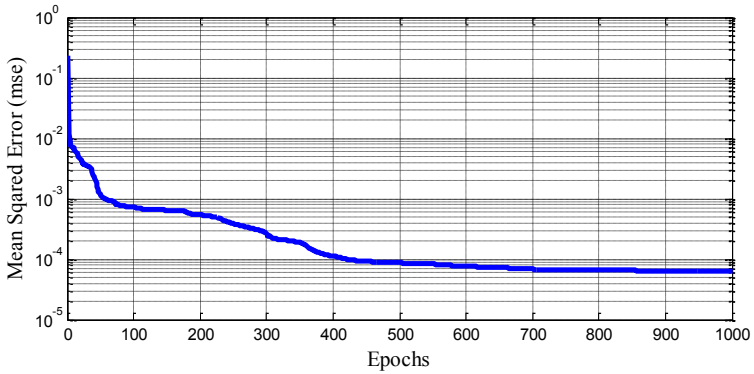

Figure 43: Lean performance of the Network using RNN.

The implemented models were compared by using the mean squared error, the hidden neuron numbers, the epoch numbers and the correlation coefficient (cc) between acquired IP²C frequency response and corresponding estimations. Results are given in Table

VII. It is possible to observe that among investigated models, the FFNN model is able to simulate in a more consistent way the frequency response of IP²C actuator.

TABLE VII: MODELS COMPARISON

	MSE	*Neurons*	*Epochs*	*cc*
FFNN	**$0.535*10^{-4}$**	**37**	**411**	**0.9978**
RBNN	0.00395	100	248	0.8904
RNN	$0.628*10^{-4}$	45	1000	0.9879

Conclusion

In this thesis the white box modeling of IPMC and IP²C actuators has been considered. The multiphysics models that include and integrate electrical, mechanical, chemical and thermal physics domains and their coupling effects have been introduced. As a novelty, the multi-physics domain models have been developed by using experimental deformation data and an ad-hoc optimization procedure that allowed to fit the models estimation on experimental data. The optimization algorithm implemented for parameter identification is a general tool that provides a new methodology for the characterization of new smart materials' properties where the physics parameters are yet not well characterized and sometime difficult to obtain from measurements.

The validation of the models is reported and adherence with recorded data is shown, identifying a second-order-like dynamics and the frequency response.

Moreover, another model of IP²C actuator based on neural network modeling has been presented. That activity was focused on the investigation of IP²C dynamic behavior in the frequency domain, taking into account the effect of humidity. This model was intended as proof of concept of the possibility to explain vibrating

structures to realize polymeric sensors.

Concluding, the proposed models allow thus to estimate a number of microscopic and macroscopic quantities involved in the study of actuators so that it can improve the comprehension of such a complex device and can represent a suitable tool for people involved characterization and synthesis new transducing polymeric devices.

Bibliography

[1] Y. Bar-Cohen, 2004, Electroactive Polymer (EAP) Actuators as Artificial Muscles-reality, potential and challenges, 2nd edition*, SPIE Press*, 2004

[2] Shahinpoor M and Kim KJ 2001, Ionic polymer–metal composites: I. Fundamentals *Smart Mater Struct.* 10 819–33

[3] Shahinpoor M, Bar-Cohen Y, Simpson Y O and Smith J, 1998, Ionic polymer–metal composites (IPMC) as biomimetic sensors, actuators, and artificial muscle - a review *Smart Mater.Struct.* 7 R15–30

[4] Shainpoor M and Kim KJ Ionic polymer-metal composites: IV. 2005 Industrial and medical applications *Smart Mater Struct.* 14 197-214

[5] Chu W-S, Lee K-T, Song S-H, Han M-W, Lee J-Y, Kim H-S, Kim M-S, Park Y-J, Cho KJ and Ahn S-H, Review of Biomimetic Underwater Robots Using Smart Actuators 2012 *Int. J of Prec. Eng. and Manuf.* 7 1281-1292.

[6] Pugal D, Jung K, Aabloo A and Kim KJ 2009 Ionic polymer-metal composite mechanoelectrical tranduction: review and perspectives *Polym. Int.* 59 279-289

[7] Di Pasquale G, Fortuna L, Graziani S, La Rosa M, Nicolosi D, Sicurella G, Umana E, All-organic motion sensors: characterization and modeling, *IEEE Trans. Instrum. Meas* (I2MTC'08 Special Issue), Vol. 58, 10, Oct. 2009, pp.3731-3738

[8] Bhandari B, Lee GY, Ahn SH 2012 A Review on IPMC Material as Actuators and Sensors: Fabrications, Characteristics and Applications *Int. J. Precision Eng. Manufact.* 13 141–163.

[9] Zhu Z, Chen H, Chang L, and Li B, 2011, Dynamic model of ion and water transport in ionic polymer-metal composites *AIP Advances* 1 040702-1-040702-14

[10] De Gennes PG, Okumura K, Shahinpoor M and Kim KJ 2000 *Europhysics Letters* 50 (4) 513-518

[11] Asaka K and Oguro K 2000 Bending of polyelectrolyte membrane platinum composites by electric stimuli: Part II. Response kinetics *Journal of Electroanalytical Chemistry* 480 (1-2) 186-198

[12] Shahinpoor M 2003 Ionic polymer-conductor composites as biomimetic sensors, robotic actuators and artificial muscles - a review *Electrochimica Acta* 48 (14-16) 2343-2353

[13] Paquette JW, Kim KJ and Kim D 2005 Low temperature characteristics of ionic polymer–metal composite actuators *Sensors and Actuators A: Physical* 118 (1) 135-143

[14] McGee JD 2002 Dissertation Mechano-electrochemical Response of Ionic Polymer-metal Composites, University of California

[15] Auclair A, Nikonenko V, Larchet L, Métayer M and Dammak L 2002 Correlation between transport parameters of ion-exchange membranes *Journal of Membrane Science* 195 (1) 89-102

[16] Mulder M 1996 *Basic Principles of Membrane Technology* Second Edition, Kluwer Academic Publishers

[17] Tadokoro S, Yamagami S, Takamori S and Oguro K 2000 Modeling of Nafion-Pt composite actuators (ICPF) by ionic motion Proc. SPIE 3987 92-102

[18] Toi Y and Kang SS, 2005, Finite element analysis of two-dimensional electrochemical-mechanical response of ionic

conducting polymer-metal composite beams Computers & Structures 83 (31-32) 2573-2583

[19] Gong Y Tang C-y, Tsui C-p and Fan J 2009 Modelling of ionic polymer-metal composites by a multi-field finite element method International *Journal of Mechanical Sciences* 51 741-751

[20] Branco PJC and Dente JA 2006 Derivation of a continuum model and its electric equivalent-circuit representation for ionic polymer-metal composite (IPMC) electromechanics *Smart Materials and Structures* 15 (2) 378-392

[21] Tatsuya Yamaue H M, Asaka K and Doi M 2005 Electrostress Diffusion Coupling Model for Polyelectrolyte Gels *Macromolecules* 38 (4) 1349-1356

[22] Nemat-Nasser S and Jiang Yu L 2000 Electromechanical response of ionic polymer-metal composites *Journal of Applied Physics* 87 (7), 3321-3331

[23] Nemat-Nasser S, 2002 Micromechanics of Actuation of Ionic Polymer-metal Composites *Journal of Applied Physics* 92 (5) 2899-2915

[24] Farinholt K and Leo DJ 2004 Modeling of electromechanical charge sensing in ionic polymer transducers *Mechanics of Materials* 36 (5-6) 421-433

[25] Farinholt K and Leo DJ 2008 Modeling the electrical impedance response of ionic polymer transducers *Journal of Applied Physics* 104 014512

[26] Chen Z, Tan XB, Will A and Ziel C 2007 A dynamic model for ionic polymer–metal composite sensors *Smart Materials and Structures* 16 1477-1488

[27] Chen Z, Hedgepeth DR and Tan XB 2009 A nonlinear, control-oriented model for ionic polymer–metal composite actuators *Smart Materials and Structures* 18 055008

[28] Choonghee J, Naguib HE and Kwon RH 2008 Modeling and optimization of the electromechanical behavior of an ionic polymer–metal composite *Smart Materials and Structures* 17 065022

[29] Johnson T, Amirouche F, 2008, Multiphysics modeling of an IPMC microfluidic control device Microsoft Technol. 14 (6) 871-879

[30] Pugal D, Kim KJ and Aabloo A, 2011, An explicit physics-based model of ionic polymer-metal composite actuators *Journal of Applied Physics* 110 084904

[31] Nemat-Nasser S and Zamani S, 2006, Modeling of electrochemomechanical response of ionic polymer-metal composites with various solvents *Journal of Applied Physics* 100 064310

[32] Porfiri M, 2008, Charge dynamics in ionic polymer metal composites *Journal of Applied Physics* 104 104915

[33] Aureli M and·Porfiri M, 2013, *Nonlinear sensing of ionic polymer metal composites Continuum Mech. Thermodyn.* 25 273–310

[34] Wallmersperger T, Leo DJ and Kothera CS, 2007, Transport modeling in ionomeric polymer transducers and its relationship to electromechanical coupling *Journal of Applied Physics* 101 024912

[35] Nardinocchi P and Pezzulla M, 2013, Curled actuated shapes of ionic polymer metal composites strips, *J. of Appl. Physics* 113 224906

[36] Galante S, Lucantonio A and Nardinocchi P, 2013, The multiplicative decomposition of the deformation gradient in

the multiphysics modeling of ionic polymers *International Journal of Non-Linear Mechanics* 51 112–120

[37] Zhang L and Yang YW, 2007, Modeling of ionic polymer-metal composite beam on human tissues *Smart Materials and Structures* 16 (2) S197-S206

[38] Del Bufalo G, Placidi L and Porfiri M, 2008, A mixture theory framework for modeling the mechanical actuation of ionic polymer metal composites, *Smart Materials and Structures* 17(4) 045010

[39] Porfiri M, 2009, An electromechanical model for sensing and actuation of ionic polymer metal composites, *Smart Materials and Structures* 18 015016

[40] http://www.comsol.com/

[41] Pugal D, Solin P, Kim KJ and Aabloo A, 2012, Modeling ionic polymer–metal composites with space-time adaptive multimesh hp-FEM *Communications in Computational Physics* 11 249–270

[42] Jong Yoon W, Reinhall G and Seibel EJ, 2007, Analysis of electro-active polymer bending: A component in a low cost

ultrathin scanning endoscope Sensor and Actuator, A 133 506–517

[43] Lughmani WA, Jho JY, Lee JY and Rhee JYK, 2009, Modeling of bending behavior of IPMC beams using concentrated ion boundary layer, *International Journal Of Precision Engineering And Manufacturing* 10(5) 131–139

[44] Samaranayake BGLT, Preethichandra DMG, Alahakoon AMUSK and Kaneto K, 2007, Modeling Simulation and Design of Ionic Polymer Metal Composite Soft Actuators *Second International Conference on Industrial and Information Systems, ICIIS* 8–11.

[45] Aldrich Technical Information Bulletin AL-163, Nafion® Resins.

[46] Higgins S J, Lovell K V, Rajapakse R M G and Walsby N M, 2003, Grafting and electrochemical characterisation of poly-(3,4-ethylenedioxythiophene) films, on Nafion and on radiation-grafted polystyrenesulfonate–polyvinylidene fluoride composite surfaces, *J. Mater. Chem.*, 13, , pp. 2485-2489.

[47] Fortuna L, Graziani S, La Rosa M, Nicolosi D, Sicurella G, Umana E, 2009, Modeling and design of all-organic

electromechanic transducers", *IS-FOE'08 special issue*, Eur Phys J-Appl Phys, vol.46, no.1, pp.12513 (p1-p4).

[48] Nemat-Nasser S and Zamani S 2003 Experimental study of Nafion- and Flemion-based ionic polymer metal composites (IPMCs) with ethylene glycol as solvent *Smart Structures and Materials 2003: Electroactive Polymer Actuators and Devices* 5051, ed Y Bar-Cohen 233–44.

[49] Caponetto R, De Luca V, Graziani S, Sapuppo F and Umana E 2012 A Multi-Physics Model of an IPMC Actuator in the Electrical, Chemical, Mechanical and Thermal Domains *SMACD 2012* 18-21

[50] Caponetto R, De Luca V, Di Pasquale G, Graziani S, Sapuppo F, and Umana E. (2013, May). A new multi-physics model of an IP²C actuator in the electrical, chemical, mechanical and thermal domains. In *Instrumentation and Measurement Technology Conference (I2MTC), 2013 IEEE International* (pp. 971-975). IEEE.

[51] Pugal D, Kasemägi H, Kim KJ, Kruusmaa M and A. Aablo 2007 Finite element simulations of the bending of the IPMC sheet Proceedings of International Society For Optical Engineering (SPIE) (EAPAD)

[52] Wilson E 2004 Static and Dynamic Analysis of Structures, 4th Edition, (231, section "Stiffness and Mass Proportional Damping")

[53] Jo C, Pugal D, Oh IK, Kim KJ and Asaka K 2013 Recent advances in ionic polymer-metal composite actuators and their modeling and applications Progress in Polymer Science 38 1037-1066.

[54] Menard KP 1999 Dynamic Mechanical Analysis: A Practical Introduction Boca Raton: CRC Press.

[55] Di Pasquale G, Graziani S, La Rosa M, Sicurella G and Umana E, 2013 IP²C Sensor Modeling *IEEE Transactions on Instrumentation and Measurement* 62 (5) 1284-1291.

[56] Caponetto R, De Luca V, Graziani S, and Sapuppo F, 2013, An optimized frequency-dependent multiphysics model for an ionic polymer–metal composite actuator with ethylene glycol as the solvent. *Smart Materials and Structures*,*22*(12), 125016.

[57] Caponetto R, De Luca V, Di Pasquale G, Graziani S, Sapuppo F and Umana E, 2014, A Multiphysics Frequency-Dependent Model of an IP²C Actuator, *IEEE Transactions on Instrumentation and Measurement* 63 (5) 1347-1355 .

[58] Newbury KM and Leo DJ 2003 Linear Electromechanical Model of Ionic Polymer Transducers – Part I: Model Development *J. of Intelligent Material Systems and Structures* 14 333 342.

[59] Nelder J A and Mead R, A simplex method for function minimization, 1965, *The Computer Journal* 7 (4): 308-313.

[60] Cha Y, Aureli M, Porfiri M. 2012 A physics-based model of the electrical impedance of ionic polymer metal composites, *Journal of Applied Physics* 111(2), 124901

[61] Cha Y, Porfiri M. 2013 A bias-dependent model of the electrical impedance of ionic polymer metal composites, *Physical Review E* 87(2), 022403.

[62] Akle B J., Habchi W., Wallmersperger T., Akle E. J., and Leo D. J. 2011 High surface area electrodes in ionic polymer transducers: Numerical and experimental investigations of the electro-chemical behavior*, Journal of Applied Physics* ,109 074509

[63] Kanno R, Tadokoro S, Takamori T, Hattori M, and Oguro K (1995, November). Modeling of ICPF (ionic conducting polymer film) actuator-modeling of electrical characteristics. In Industrial Electronics, Control, and Instrumentation,

Proceedings of the 1995 IEEE IECON 21st International Conference on (Vol. 2, pp. 913-918).

[64] Caponetto R, Dongola G, Fortuna L, Graziani S, and Strazzeri S (2008, May). A fractional model for IPMC actuators. In *Instrumentation and Measurement Technology Conference Proceedings. IMTC 2008. IEEE*(pp. 2103-2107). IEEE.

[65] Caponetto R, Graziani S, Pappalardo F L, and Sapuppo F (2013). Experimental characterization of ionic polymer metal composite as a novel fractional order element. *Advances in Mathematical Physics*, *2013*.

[66] Krishna M S, Das S, Biswas K, and Goswami B (2009, November). Characterization of a fractional order element realized by dipping a capacitive type probe in polarizable medium. In *Proceedings of the Symposium on Fractional Signals and Systems, Lisbon'09* (pp. 4-6).

[67] Caponetto R, De Luca V., Graziani S, Sapuppo F, and Di Pasquale G. (2014, May). IPMC frequency dependent multiphysics model considering electrodes high surface and fractional effects. In *Instrumentation and Measurement Technology Conference (I2MTC) Proceedings, 2014 IEEE International* (pp. 1529-1532). IEEE..

[68] R. Caponetto, V. De Luca, G. Di Pasquale, S. Graziani, A layered mutiphysics white box model of IPMC actuators , *I2MTC 2015*, Pisa, submitted.

[69] R. Caponetto, V. De Luca, S. Graziani, A Multiphysics model of IPMC actuators dependence on relative humidity, *I²MTC 2015*, Pisa, accepted.

[70] Brunetto P, Fortuna L, Giannone P, Graziani S, and Strazzeri S (2010). Static and dynamic characterization of the temperature and humidity influence on IPMC actuators. *Instrumentation and Measurement, IEEE Transactions on*,*59*(4), 893-908.

[71] Brunetto P, Fortuna L, Giannone P, Graziani S, and Strazzeri S (2011). Characterization of the temperature and humidity influence on ionic polymer–metal composites as sensors. *Instrumentation and Measurement, IEEE Transactions on*, *60*(8), 2951-2959.

[72] De Luca V, Hossaini-Asl E, Graziani S, Zurada J M, 2014, Neural modeling of relative humidity on IP²C vibrating transducer, *Eurosensors 2014*.

[73] Stinchcombe M, and White H (1989, June). Universal approximation using feedforward networks with non-sigmoid

hidden layer activation functions. In*Neural Networks, 1989. IJCNN., International Joint Conference on* (pp. 613-617). IEEE.

[74] Park, J., and Sandberg, I. W. (1991). Universal approximation using radial-basis-function networks. *Neural computation*, *3*(2), 246-257.

[75] Elman J L (1990). Finding structure in time. *Cognitive science*, *14*(2), 179-211.